J Neurophysiol 100: 852–867, 2008.
First published May 28, 2008; doi:10.1152/jn.90300.2008.

Temporal Processing Across Multiple Topographic Maps in the Electrosensory System

Rüdiger Krahe,[1] Joseph Bastian,[3] and Maurice J. Chacron[2]

[1]*Department of Biology and* [2]*Department of Physiology, Center for Nonlinear Dynamics, McGill University, Montreal, Quebec, Canada; and* [3]*Department of Zoology, University of Oklahoma, Norman, Oklahoma*

Submitted 24 February 2008; accepted in final form 21 May 2008

Krahe R, Bastian J, Chacron MJ. Temporal processing across multiple topographic maps in the electrosensory system. *J Neurophysiol* 100: 852–867, 2008. First published May 28, 2008; doi:10.1152/jn.90300.2008. Multiple topographic representations of sensory space are common in the nervous system and presumably allow organisms to separately process particular features of incoming sensory stimuli that vary widely in their attributes. We compared the response properties of sensory neurons within three maps of the body surface that are arranged strictly in parallel to two classes of stimuli that mimic prey and conspecifics, respectively. We used information-theoretic approaches and measures of phase locking to quantify neuronal responses. Our results show that frequency tuning in one of the three maps does not depend on stimulus class. This map acts as a low-pass filter under both conditions. A previously described stimulus-class-dependent switch in frequency tuning is shown to occur in the other two maps. Only a fraction of the information encoded by all neurons could be recovered through a linear decoder. Particularly striking were low-pass neurons the information of which in the high-frequency range could not be decoded linearly. We then explored whether intrinsic cellular mechanisms could partially account for the differences in frequency tuning across maps. Injection of a Ca^{2+} chelator had no effect in the map with low-pass characteristics. However, injection of the same Ca^{2+} chelator in the other two maps switched the tuning of neurons from band-pass/high-pass to low-pass. These results show that Ca^{2+}-dependent processes play an important part in determining the functional roles of different sensory maps and thus shed light on the evolution of this important feature of the vertebrate brain.

INTRODUCTION

Sensory systems have to process stimuli covering a large range of spatiotemporal characteristics. A possible solution to this problem is to devote specific neural circuits to detect particular subsets of incoming stimuli. This solution appears to be favored as many systems have multiple representations of the same sensory space by different neural populations, thereby allowing each representation to focus on a subset of behaviorally relevant stimuli (MacLeod and Carr 2007; Wässle 2004). However, the mechanisms that enable sensory neurons in different maps to respond to different features of the sensory environment are poorly understood and difficult to address in systems with complex lateral and hierarchical connectivity (Graziano and Aflalo 2007; Van Essen and Gallant 1994). The electrosensory system of weakly electric fish offers a unique window into this problem because it contains three somatotopic maps that are arranged strictly in parallel, have nearly identical neural circuitry, and receive exactly the same pattern of receptor afferent inputs (Berman and Maler 1999).

Weakly electric fish generate an electric field (electric organ discharge, EOD) around themselves and sense perturbations of this field caused by nearby objects, such as prey, or by the EODs of conspecifics (Chacron 2007; Fortune 2006; Fortune et al. 2006; Nelson and MacIver 1999). These perturbations cast electric images onto the skin where tuberous electroreceptor organs respond to changes in EOD amplitude. Primary afferents carry this information to the electrosensory lateral line lobe (ELL) of the hindbrain (Scheich et al. 1973). Each afferent fiber trifurcates sending one collateral to each of three somatotopic representations of the body surface in the ELL: the centromedial segment (CMS), centrolateral segment (CLS), and lateral segment (LS) (Heiligenberg and Dye 1982) (Fig. 1, *A* and *B*). A fourth map, the medial segment (MS) is formed by input from ampullary electrosensory afferents and will not be discussed further. Pyramidal cells are the sole amplitude-coding output neurons of the three maps. Two basic cell types are found in each of the maps: E-cells respond to increases in EOD amplitude and I-cells respond to decreases in amplitude, analogous to ON and OFF cells in the visual system (Krahe and Gabbiani 2004; Maler et al. 1981; Saunders and Bastian 1984).

Weakly electric fish process sensory stimuli with a wide range of spatiotemporal characteristics. *1*) Electric images caused by objects in the environment, such as prey, plants, or rocks, typically contain low frequencies ($<$15 Hz) and are spatially localized to a fraction of the animal's skin surface (Nelson and MacIver 1999). *2*) In contrast, electric images encountered during interactions with conspecifics are spatially diffuse and can contain low temporal frequencies typical of same-sex interactions as well as high frequencies characteristic of opposite-sex interactions ($\leq$350 Hz). Stimuli of high temporal frequency are also caused by brief frequency modulations of the electric organ discharge (EOD) (Kelly et al. 2008; Zakon et al. 2002; Zupanc and Maler 1993). Pyramidal cells within the different segments receive identical afferent input from the electroreceptive skin surface (Heiligenberg and Dye 1982). In the distantly related genus *Eigenmannia*, the pyramidal cells of the three segments have been shown to differ in the sizes of their receptive fields and to be tuned to different temporal frequencies of spatially diffuse sensory stimuli (Metzner et al. 1998; Shumway 1989a,b). Cells of the CMS had small receptive fields and responded best to amplitude modulations (AMs) of low frequency, whereas pyramidal neurons of the LS had the

Address for reprint requests and other correspondence: R. Krahe, Dept. Biology, McGill University, 1205 Ave. Docteur Penfield, Montreal, QC H3A 1B1, Canada (E-mail: rudiger.krahe@mcgill.ca).

The costs of publication of this article were defrayed in part by the payment of page charges. The article must therefore be hereby marked "*advertisement*" in accordance with 18 U.S.C. Section 1734 solely to indicate this fact.

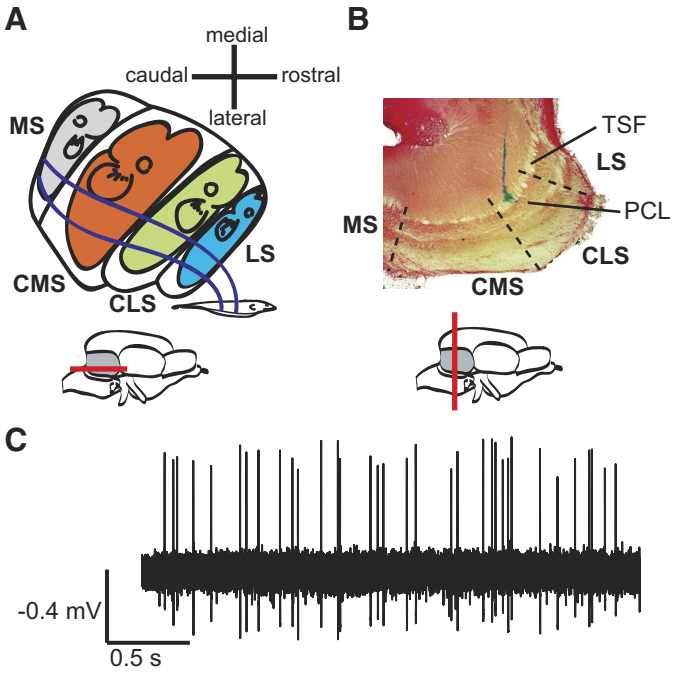

FIG. 1. The electrosensory lateral line lobe (ELL) contains 4 topographic maps of the body surface. *A*: sketch of a horizontal section through the right ELL showing the oblique orientation of the maps and the topographic relationship with the skin surface. *Inset*: lateral view of the brain with the ELL shown in gray. The red line indicates the dorsoventral level of the horizontal section. The medial segment (MS) receives input from ampullary electroreceptors, whereas the other 3 segments receive input from tuberous electroreceptors (CMS, centromedial segment; CLS, centrolateral segment; LS, lateral segment). The "pisciculi" of MS and CMS and of CLS and LS abut ventrally, the maps of CMS and CLS abut dorsally (after Carr et al. (1982). *B*: coronal section through the right ELL at the level indicated in the *inset* showing an example of an Alcian-Blue-stained recording site in CLS at the level of the tractus stratum fibrosum (TSF). The somata of the pyramidal cells are located in the pyramidal cell layer (PCL). *C*: example trace of an extracellular recording from a pyramidal cell. The large baseline noise is due to contamination of the recording with the fish's electric organ discharge (EOD) signal.

largest receptive fields and acted as high-pass filters of AMs. CLS cells showed intermediate receptive field sizes and mostly broadband temporal filtering (Shumway 1989a). This differential processing furthermore appears to be directly related to specific behaviors: the CMS was necessary and sufficient to elicit a jamming avoidance response, which consists of the fish increasing its EOD frequency if a nearby conspecific has a frequency slightly lower than its own (<20 Hz) and of decreasing its EOD frequency if the neighbor's EOD frequency is slightly higher than its own (Metzner and Juranek 1997). The LS, on the other hand, was found to be necessary and sufficient for responding to conspecific EODs with the generation of brief frequency modulations (Metzner and Juranek 1997).

The well-characterized ELL circuitry, and the growing knowledge about pyramidal cell responses to sensory input and molecular differences in the distributions of receptors and ion channels across the segments (Berman and Maler 1999; Chacron 2006; Chacron et al. 2003, 2005b; Ellis et al. 2007; Mehaffey et al. 2006; Rashid et al. 2001) provide an opportunity to connect variations in intrinsic properties of nerve cells with the specific roles of multiple topographic representations in behavior.

METHODS

Animals and surgery

In vivo recordings were performed on 21 Brown Ghost Knifefish (*Apteronotus leptorhynchus*, Gymnotiformes) that were between 12 and 20 cm in length using previously described techniques (Bastian et al. 2002). The animals were housed in 150-l tanks at a temperature between 26 and 28°C. The conductivity of the tank water ranged between 200 and 1,000 μS; pH was maintained between 6.8 and 7.2. The experiments were performed in Plexiglas tanks (30 × 30 × 10 cm) filled with water from the respective fish's home tank. The animals were immobilized by intramuscular injection of 4 mg of the nicotinic receptor antagonist Tubocurarine (Sigma, St. Louis, MO) and respirated via a mouth tube with aerated tank water at a flow rate of 10 ml/min. The fish was submerged in water except for the top of its head. To expose the hindbrain for recording, we first locally anesthetized the skin on the skull by applying 2% Lidocaine. Then we removed ~6 mm^2 of skin to expose the skull to which a metal post was glued for stabilization. By drilling a hole of ~2 mm^2, we gained access to the area of the cerebellum overlying the ELL. The surface of the brain was kept covered by saline (Bastian 1974) throughout the experiment. Animal care and all surgical procedures were in accordance with the University of Oklahoma animal care and use guidelines.

Recording

Extracellular single-unit recordings from 65 pyramidal cells were made with double-barrel electrodes, one barrel of which had been filled with Wood's metal and the tip plated with gold and platinum for recording (Frank and Becker 1964) (Fig. 1*C*). The second barrel was filled with a 1% solution of Alcian Blue (Sigma) to allow marking of the recording sites (Fig. 1*B*). Intracellular recordings from 28 pyramidal cells were made with thin-walled borosilicate glass micropipettes (Sutter Instruments, Novato, CA) filled with 3 M KCl. To disrupt intracellular Ca^{2+} signaling, the tips of the micropipettes were filled with 100 mM 1,2-bis (2-aminophenoxy)ethane-*N*,*N*,*N*′,*N*′-tetraacetic acid (BAPTA) in 3 M KCl (Bastian 1998). The spike trains were digitized at 10 kHz using CED 1401-plus hardware and SpikeII software (Cambridge Electronic Design, Cambridge, UK). Extracellularly recorded spikes were detected with a threshold criterion and a spike-clustering algorithm; intracellularly recorded spikes were detected with a threshold criterion.

Histology

To assign each of the recorded pyramidal cell responses to one of the three segments of the ELL, Alcian Blue was pressure-ejected (Picospritzer II, General Valve, Fairfield, NJ) from the second barrel of the recording electrode once the physiological characterization of the given cell had been completed. In a given fish, we recorded from up to six pyramidal cells (3 on each side of the brain) and marked the recording sites. On completion of the experiment, the fish was deeply anesthetized by injection of Ketamine (0.5 ml of 100 ppm solution; Sigma), and perfused through the heart with 4% glutaraldehyde followed by 4% glutaradehyde in 30% sucrose. After overnight postfixation, the frozen brain was sectioned (60 μm) and counterstained with Pyronin Yellow. These stains typically allowed unambiguous assignment of recording sites to the ELL segments (Fig. 1*B*). Cases in which no unambiguous assignment to one of the segments could be made (insufficient staining or mark exactly on the boundary between two segments) were discarded from the analysis.

Pharmacology

Previously established micropressure ejection techniques were used to focally apply glutamate (Glu, 1 mM), iberiotoxin (IBTX, 1 mM, $n = 7$), apamin (1 mM, $n = 18$), and 1-ethyl-2-benzimidazolinone (EBIO, 1 mM, $n = 5$) within the ELL molecular layer containing the

apical dendritic trees of a given cell (Bastian 1993; Bastian and Nguyenkim 2001; Bastian et al. 2004; Chacron 2006; Chacron and Bastian 2008; Chacron et al. 2005b). The agents were dissolved in distilled water (Bastian 1993). Multibarrel pipettes were pulled to a fine tip and subsequently broken to a total tip diameter of 10 μm. One barrel was filled with Glu, while the remaining barrels were filled with one or more of the other solutions. Once an extracellular recording from a pyramidal cell was established, the multibarrel pipette was slowly advanced into an appropriate region of the ELL molecular layer while periodically ejecting "puffs" of Glu (duration = 100 ms, pressure = 40 psi). As described previously, proximity to the apical dendrite of a recorded cell will result in short-latency excitation of that cell (Bastian 1993). After satisfactory placement, each drug was delivered by a series of pressure pulses (duration = 100 ms, pressure = 40 psi). Drugs were purchased from Sigma (St. Louis, MO) and Tocris (Ellisville, MO).

Stimulation

The EOD persists after immobilization with the curare-like drug because the electric organ of *Apteronotus* is neurogenic. Therefore all stimuli consisted of modulations of the fish's own EOD by electric signals applied either globally via chloridized silver wire electrodes positioned 19 cm away from the fish on either side of the animal or locally via a small local dipole electrode positioned 2–4 mm from the skin (Bastian et al. 2002). The fish's EOD was recorded with chloridized silver wire electrodes positioned at the head and at the tail. The zero crossings of the amplified EOD signal (DAM50, World Precision Instruments, Sarasota, FL; band-pass filter between 300 Hz and 3 kHz) were detected by a window discriminator, which then triggered a function generator to output a single-cycle sinusoid of slightly higher frequency than the fish's EOD. This created a train of single-cycle sinusoids that were phase-locked to the EOD. The train was then multiplied (MT3 multiplier, Tucker Davis Technologies, Gainesville, FL) with a modulation waveform produced by Labview 7 (National Instruments, Austin, TX) and D/A converted by a DAQCard-6715 board (National Instruments). The resulting signal was attenuated (LAT45 attenuator, Leader Electronics, Cypress, CA) and fed into the tank via a stimulus isolator (A395 linear stimulus isolator, World Precision Instruments). Depending on the polarity of the signal relative to the fish's EOD, the signal led to an increase or a decrease in amplitude of the EOD.

We characterized neuronal activity under baseline conditions, with no external stimulus provided and the electrosensory system being driven solely by the fish's unmodulated EOD, and under driven conditions. To drive the electrosense, we used sinusoidal amplitude modulations (SAMs) at discrete frequencies ranging from 5 to 120 Hz, random amplitude modulations (RAMs), and step changes in EOD amplitude. The modulation waveform for the RAMs was a low-pass-filtered (8th-order Butterworth filter, cutoff frequency: 120 Hz), zero-mean, Gaussian noise. The stimulus consisted of a 20-s-long noise segment that was repeated four times. The step stimuli were of 100-ms duration and were repeated $\geq$30 times to obtain sufficient amounts of data. The amplitude of the global stimulus was calibrated at the position usually occupied by the fish but measured without the fish being in place. The reference amplitude at 0 dB was set to 1 mV/cm. Typical attenuation levels for global stimulation were -20 to -25 dB, for local stimulation, -15 to -20 dB. This setting for the local stimulus relative to the global stimulus was shown to provide equivalent drive to primary electrosensory afferents (Bastian et al. 2002). The modulation waveforms were sampled at 2 kHz.

Data analysis

Spontaneous pyramidal cell activity was accumulated as a sequence of spike times for each cell. Spike trains were binned into 0.5-ms bins that contained at most one spike as done previously (Bastian et al. 2002; Chacron and Bastian 2008; Chacron et al. 2003, 2005a,b). We then computed the autocorrelogram of each cell's activity as $A(\tau) = \langle X(t)\, X(t+\tau)\rangle$ with a bin width of $dt = 1$ ms. Here the averaging $\langle \ldots \rangle$ is performed over time t. We then used the autocorrelogram to determine an interspike interval (ISI) threshold criterion as done previously (Bastian and Nguyenkim 2001). Briefly we determined the expected content of bin i for a Poisson process from $y = fN\,dt$, where f is the firing rate and N is the number of spikes. The upper limit of the 99% confidence interval around y was then computed (Abeles 1982; Bastian and Nguyenkim 2001), and we took the ISI threshold as the time at which the falling phase of the initial autocorrelogram peak crossed that limit. This ISI threshold was then used to compute the burst fraction (BF), which is defined as the fraction of ISIs that are lower than the threshold (Oswald et al. 2004).

Responses to SAMs were accumulated as phase histograms, and responses were quantified as the vector strength or mean vector length (Mardia and Jupp 1999). This measure ranges from 0, when there is no phase relationship between the stimulus and response, to 1 with perfect phase locking. We also applied a recently developed measure based on the entropy of the phase histogram of the response, which is less sensitive to deviations from unimodality in phase histograms than the vector strength (Kajikawa and Hackett 2005). The results were qualitatively the same as the ones based on vector strength (data not shown), which is to be expected because phase histograms from pyramidal cells are generally unimodal (Bastian 1981b; Bastian et al. 2002).

Responses to RAMs were accumulated as sequences of spike times for each cell. The data analysis and stimulation protocols were similar to those used previously (Chacron 2006). Briefly, the four spike trains obtained in response to repeated presentations of the same stimulus waveform S, each lasting 20 s, were labeled R_1–R_4. We computed the cross-spectrum $SR_i(f)$ between the stimulus S and spike train R_i, the stimulus power spectrum $SS(f)$, and the power spectrum $RR_i(f)$ of spike train R_i. All these quantities were computed using multitaper estimation techniques with eight Slepian sequences (Jarvis and Mitra 2001). A lower bound on the rate density of information transmission at frequency f can be computed from the stimulus-response (SR) coherence (Borst and Theunissen 1999; Marsat and Pollack 2004; Rieke et al. 1996) as $I_{\text{lower}}(f) = -\log_2(1 - C_{SR}(f))$ where $C_{SR}(f)$ is the stimulus response coherence given by

$$C_{SR}(f) = \frac{\left|\frac{1}{4}\sum_{i=1}^{4} SR_i(f)\right|^2}{\frac{SS(f)}{4}\sum_{i=1}^{4} RR_i(f)}$$

The total information rate MI_{lower} is obtained by integrating $I_{\text{lower}}(f)$ between 0 and the stimulus' cutoff frequency f_c.

Roddey et al. (2000) have proposed a method for assessing the performance of neural encoding models: the performance of the best linear model can be assessed by the SR coherence. However, nonlinear models can outperform linear ones and the response-response (RR) coherence gives an upper bound on the performance of the optimal nonlinear model. A comparison between the SR coherence and the square root of the RR coherence will thus quantify the performance of the best linear model with respect to the optimum performance theoretically achievable. The RR coherence is given by (Roddey et al. 2000)

$$C_{RR}(f) = \frac{\left|\frac{1}{6}\sum_{i=1}^{4}\sum_{j<i} RR_{ij}(f)\right|^2}{\left(\frac{1}{4}\sum_{j=1}^{4} RR_i(f)\right)^2}$$

where RR_{ij} is the cross-spectrum between spike trains R_i and R_j. An upper bound on the information rate can be obtained from the

response-response coherence from $I_{upper}(f) = -\log_2\{1 - C_{RR}(f)^{1/2}\}$ (Borst and Theunissen 1999; Chacron 2006; Marsat and Pollack 2004). An upper bound on the total information rate is then obtained by integrating $I_{upper}(f)$ between 0 and f_c.

Statistical analysis was performed using the Matlab Statistics Toolbox. When an ANOVA indicated significant differences between ELL segments, the Tukey-Kramer post hoc test was used for pairwise comparisons. Prior to statistical tests comparing percent values, data were arc-sine transformed.

BAPTA injection

We performed intracellular recordings with the pipette tip filled with 100 mM BAPTA. Before iontophoretically injecting the drug into the pyramidal cells, we gathered control data with a reduced stimulation protocol limited to global RAMs (four repetitions of a 20-s waveform) and the recording of spontaneous activity because BAPTA was found to passively leak into the cell. We focused on potential differences between CMS and the two more lateral ELL maps and pooled data from E- and I-cells. For intracellular recordings, we distinguished between CMS and CLS/LS in the following way: CMS cells can be targeted using anatomical landmarks and physiological mapping of the border with the medially adjoining medial segment the neurons of which exclusively respond to low-frequency carrier signals but not to amplitude modulations of the high-frequency EOD (Heiligenberg and Dye 1982; Metzner et al. 1998). Recordings from CLS/LS were based on recording depth and surface landmarks as previously reported (Bastian et al. 2002).

We measured the amplitude of spike afterhyperpolarization in intracellular recordings by subtracting the average membrane potential in the 2 ms following an isolated action potential from the average membrane potential preceding that same action potential. An action potential was deemed to be isolated if there were no other spikes within a window of 200 ms centered on the action potential in question.

The effects on frequency tuning we observed with BAPTA application potentially could have been due to changes in chloride reversal potential caused by leakage of chloride from our intracellular recording electrodes. Changes in the chloride reversal potential could have eliminated GABAergic inhibition and potentially affected frequency tuning (Berman and Maler 1998a,b). This is unlikely, however, because Bastian (1993) observed inhibitory effects of GABA when recording from pyramidal cells with electrodes filled with KCl and HRP. Similar intracellular responses of pyramidal cells have been recorded with K^+-acetate-filled electrodes (Middleton et al. 2006). Further, recent recordings with electrodes filled with K^+-acetate and BAPTA (N. Toporikova and M. J. Chacron, unpublished data) confirmed our findings on the changes in frequency tuning.

Pharmacological blockade of Ca^{2+}-activated K^+ currents

To identify the Ca^{2+}-activated K^+ currents involved in the BAPTA-mediated effects, we attempted to block Ca^{2+}-activated K^+ currents in vivo using previously established pharmacological techniques (Bastian 1993). We used the BK channel antagonist iberiotoxin (IBTX, $n = 7$ cells), the SK channel antagonist apamin ($n = 18$ cells), and the SK channel agonist EBIO ($n = 5$ cells). None of these drugs had a significant effect on either the firing rate or the frequency tuning of CLS/LS pyramidal cells (data not shown). Note that because our recordings were extracellular, we could not ascertain the effects of apamin, IBTX, and EBIO on the AHP or spike shape.

Modeling

We modeled pyramidal cells using a Hodgkin-Huxley-like formalism (Koch 1999). The model contains the essential spiking currents: fast inward Na^+ (I_{Na}) and outward delayed rectifying K^+ (I_{Dr}), as well as passive leak currents (I_{leak}). As well, we included a Ca^{2+} current (I_{Ca}) and a Ca^{2+}-activated K^+ current (I_{KCa}). The membrane potential V is described by

$$C_m\frac{dV}{dt} = I + \xi(t) + g_{Na}\cdot m_\infty^2\cdot(1-n)\cdot(V_{Na}-V) + S(t) + g_{Ca}\cdot m_{Ca}^2\cdot(V_{Ca}-V) + g_{Dr}\cdot n^2\cdot(V_K-V) + g_{KCa}\cdot\kappa\cdot[Ca^{2+}]\cdot(V_K-V) + g_{leak}\cdot(V_l-V)$$

I is a current bias, $S(t)$ is low-pass filtered (120-Hz cutoff, 8th-order Butterworth) noise with zero mean and SD 40, $\xi(t)$ is Gaussian white noise with zero mean and autocorrelation function $A(t,t') = 20\ \delta(t,t')$ (Gardiner 2004). Here, $[Ca^{2+}]$ is the Ca^{2+} concentration with κ a proportionality constant. The activation of spiking Na^+ in the soma, m_∞, instantaneously tracks the membrane voltage, V, and its inactivation, h, is modeled as $h \approx 1 - n$, where n is the activation parameter for I_{Dr} described by

$$\frac{dn}{dt} = \frac{n_\infty(V) - n}{\tau_n}$$

The parameter g is a maximal conductance (g_{max}, mS/cm^2), while m and s are activation parameters and h, n, and p are inactivation parameters. Each is described by the following equation

$$\frac{dx}{dt} = \frac{x_\infty(V) - x}{\tau}$$

where $x_\infty(V)$ is the infinite conductance curve and τ is the time constant. The infinite conductance curve is modeled as a sigmoid

$$x_\infty(V) = \frac{1}{1 + e^{-(V-V_{1/2})/k}}$$

using the following parameter values for $I_{Na}[m_\infty(V)]$: $g_{max} = 15$ mS/cm^2, $V_{1/2} = -50$ mV, $k = 3$; for $I_{Dr}[n(V)]$: $g_{max} = 105$ mS/cm^2, $V_{1/2} = -50$ mV, $k = 3$, $\tau = 0.19$ ms; $I_{Ca}[m_{Ca}(V)]$: $g_{max} = 0.5$ mS/cm^2, $V_{1/2} = -20$ mV, $k = 1$, $\tau = 1$ ms. The Ca^{2+} concentration follows the following equation (Wang 1998)

$$\frac{d[Ca]}{dt} = 0.0008\ g_{Ca}\cdot m_{Ca}^2\cdot(V_{Ca}-V) - \frac{[Ca]}{\tau_{[Ca]}}$$

Parameter values are: the reversal potentials: $V_{Na} = 40$ mV, $V_K = -88.5$ mV, $V_{leak} = -70$ mV; $V_{Ca} = 120$ mV; membrane capacitance: $C_m = 1\ \mu$F/cm^2; $g_{leak} = 8$ mS/cm^2; $g_{KCa} = 240$ mS/cm^2; $\kappa = 1$ M^{-1}; $\tau_{[Ca]} = 30$ ms. We used $I = 39$ and 75 for simulations without and with I_{ahp}, respectively. Spike waveform averages were obtained with $I = 27$ for both conditions.

The model equations were integrated using an Euler-Maruyama algorithm with a time step of 2.5 μs, and voltage traces obtained were analyzed in the same way as the experimental data.

RESULTS

In total, we recorded extracellularly from 65 pyramidal cells from the three maps of the ELL to describe their temporal processing characteristics. For 10 of those cells, we were unable to unequivocally assign their recording location to one of the maps (see Fig. 1*B*) and therefore excluded them from the analysis.

Spontaneous activity

Spontaneous firing rates of ELL pyramidal cells ranged from 3 to 34 Hz (Fig. 2*A*; Table 1). Although there was a slight trend

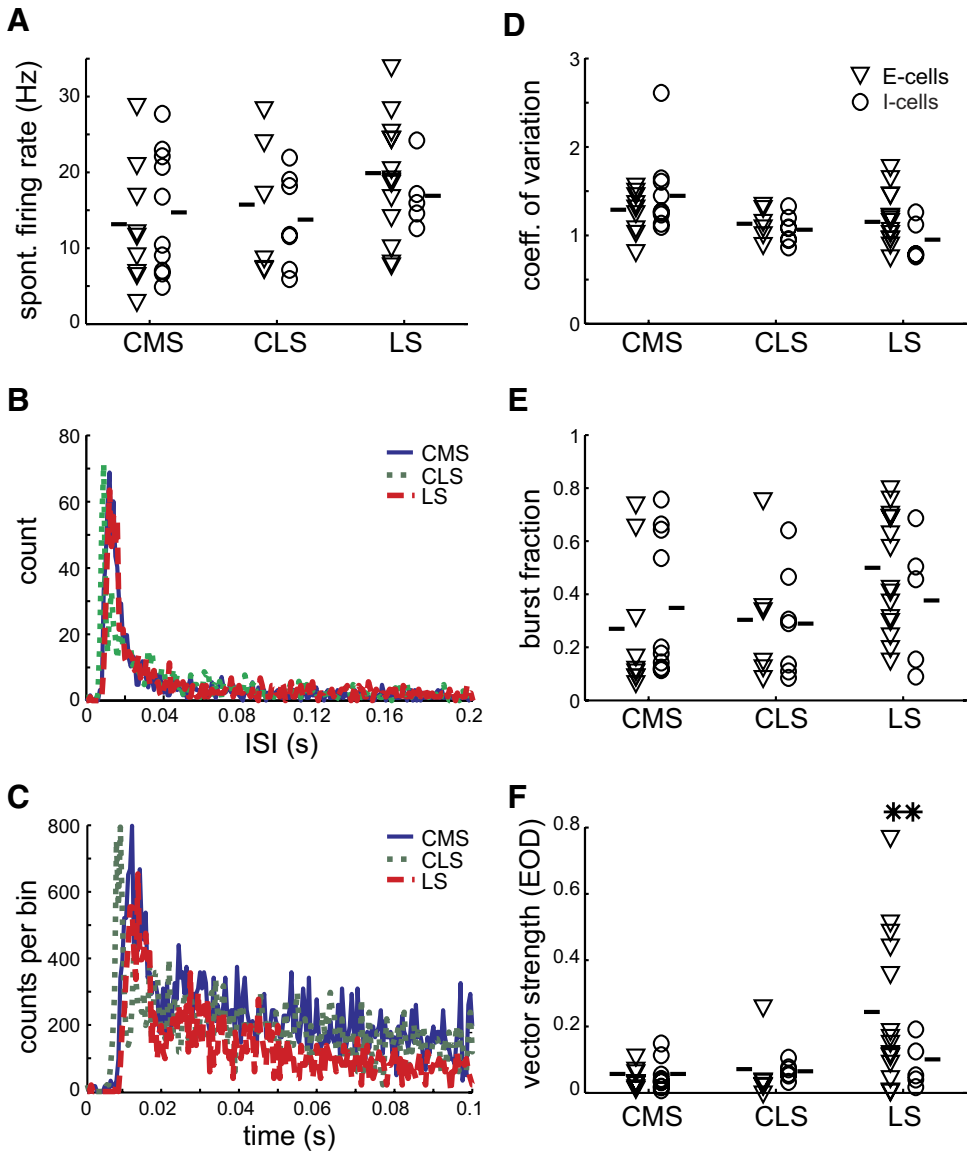

FIG. 2. Characterization of spontaneous activity of ELL pyramidal cells. *A*: spontaneous firing rates of E- and I-cells of the 3 maps. *B*: examples of interspike interval (ISI) histograms of 1 E-cell from each of the 3 maps. *C*: examples of autocorrelograms of 1 E-cell from each of the 3 maps. *D*: coefficients of variation of E- and I-cells of the 3 maps. *E*: burst fractions for E- and I-cells of the 3 maps. *F*: vector strength of E- and I-cells of the 3 maps. Triangles, E-cells; circles, I-cells. Mean values in *A*, *D*, *E*, and *F* are indicated by horizontal bars. The two asterisks in *F* indicate a statistically significant difference (*t*-test, $P < 0.01$).

for the mean firing rates of E- and I-cells to increase from CMS to CLS to LS, none of the differences between maps (1-way ANOVA; $P > 0.05$) or between E- and I-cells within maps (*t*-test: $P > 0.05$) were statistically significant. Interspike interval histograms and autocorrelograms of spontaneous activity showed the same range of variation within the different maps as across maps consistent with earlier observations (Fig. 2, *B* and *C*) (Bastian and Courtright 1991; Bastian and Nguyenkim 2001). The coefficients of variation (CVs) of the interspike intervals (ISIs) ranged from 0.76 to 2.61 (Fig. 2*D*), and the fraction of spikes assigned to spike bursts (i.e., the burst fraction) based on the autocorrelograms varied from 0.07 to 0.81 (Fig. 2*E*). The only significant difference we observed was between the CVs of I-cells in CMS and LS with the firing of LS I-cells being the most regular ($P < 0.05$). In contrast to studies performed in vitro (Mehaffey et al. 2008; Turner et al. 1996), no significant difference was seen in the amount of burst firing across cell types or maps ($P > 0.05$). Our findings on spontaneous activity are also qualitatively similar to earlier results acquired in the related weakly electric fish, *Eigenmannia*, in which, however, spontaneous activity was measured in the total absence of an

TABLE 1. *Characteristics of spontaneous activity of E-cells and I-cells of the three tuberous maps of the ELL*

	CMS-E (12)	CMS-I (16)	CLS-E (8)	CLS-I (8)	LS-E (16)	LS-I (5)
Spontaneous firing rate, Hz	13.1 ± 8.1	14.8 ± 8.2	15.7 ± 9.2	13.7 ± 6.2	19.9 ± 7.5	16.9 ± 4.4
EOD phase locking	0.05 ± 0.03	0.05 ± 0.05	0.07 ± 0.10	0.06 ± 0.02	0.24 ± 0.22	0.09 ± 0.07
CV of ISIs	1.28 ± 0.25	1.46 ± 0.45	1.15 ± 0.17	1.07 ± 0.16	1.19 ± 0.31	0.94 ± 0.23
Burst fraction	0.27 ± 0.26	0.35 ± 0.27	0.31 ± 0.25	0.29 ± 0.21	0.49 ± 0.22	0.38 ± 0.25

Values in parentheses indicate sample sizes. Spontaneous firing rates, vector strength as a measure of phase locking of spikes to the electric organ discharge (EOD), the coefficients of variation (CV) of the interspike intervals (ISIs), and the fractions of spikes fired in bursts are given as means ± SD.

EOD (Metzner et al. 1998), a situation that does not occur under natural conditions.

Phase-locking to the fish's own EOD signal was quantified using vector strength. There was a tendency for phase locking to increase from CMS over CLS to LS with the pairwise difference between CMS E-cells and LS E-cells being statistically significant ($P < 0.01$; Fig. 2*F*). Some E-cells in LS reached very high values of vector strength in the range of what is observed for primary afferent fibers (Bastian 1981a).

Mutual information

We used RAMs of the fish's EOD with a frequency range of 0–120 Hz to stimulate pyramidal cells (Fig. 3; see METHODS). We used spatially diffuse, "global", RAMs to mimic the stimuli caused by conspecifics and spatially localized, "local," RAMs to mimic the stimuli caused by prey or small objects in the environment. We then quantified the amount of information transmitted by pyramidal cells about such stimuli using information theory. We computed both lower and upper bound estimates on the amount of information transmitted as done previously (Chacron 2006; Marsat and Pollack 2004; Passaglia and Troy 2004). The lower bound estimate gives us the amount of information that can be decoded linearly from the spike train while the upper bound gives us the maximum amount of information present in theory in pyramidal cell spike trains. Thus a comparison between the two bounds allows us to quantify the contribution of nonlinear mechanisms to information transmission.

LOWER-BOUND ESTIMATE. Information transmission properties differed clearly between E-cells of the different maps (Fig. 3*A*). Our results show that the previously described switch in frequency tuning from low frequencies for local stimulation to high frequencies with global stimulation (Chacron 2006; Chacron et al. 2003, 2005b) is most pronounced in CLS. In contrast, CMS E-cells acted as low-pass filters regardless of stimulus condition, while LS E-cells acted as band-pass filters for local stimulation and band-pass to high-pass filters under global stimulation.

I-cells did not respond to high stimulus frequencies (>25 Hz) in any map for either local or global stimulation (Fig. 3*C*). Similar to previous results, I-cells of CLS showed increased responses to low frequencies for local stimulation (Chacron 2006; Chacron et al. 2005b). In contrast, CMS and LS I-cells showed no changes in frequency tuning contingent on changing the stimulus' spatial extent: good low-frequency responses were observed for both local and global geometries for CMS, while relatively poor responses were observed in LS.

To quantitatively compare frequency tuning across maps and cell types, we computed the frequency at which the information tuning curves of all recorded pyramidal cells were maximal (Fig. 4, *A* and *B*). We will first consider E-cells. For global stimulation, E-cell peak frequency generally increased from CMS over CLS to LS with the pairwise comparisons of mean peak frequencies being significant only for CMS and LS ($P < 0.01$). For local stimulation, the peak frequencies of CMS and CLS E-cells were statistically indistinguishable, and both were significantly lower than the peak frequencies of E-cells in LS ($P < 0.01$).

We did not find significant differences between I-cells of the three maps for either local or global geometry (Fig. 4*B*). Neither did we observe any significant differences in peak frequencies between E- and I-cells of the same map for either global or local stimulation (independent samples *t*-test: $P > 0.1$ for all comparisons).

When stimulation geometry was switched from global to local, all cell types showed some decrease in their peak frequency (Fig. 4, *A* and *B*). However, this decrease in best frequency was only significant for E- and I-cells of CLS and for E-cells of LS (paired *t*-test: $P < 0.05$). For LS E-cells the decrease was caused by a change in the response to high frequencies only (>20 Hz; Fig. 3*A*), whereas CLS cells changed their response to low frequencies (<20 Hz; both E- and I-cells; Fig. 3, *A* and *C*) and high frequencies (E-cells only). E- and I-cells in CMS as well as I-cells in LS did not show significant changes in this measure of their frequency tuning.

To summarize, we observed strong differences in information tuning between maps and cell types and also in how frequency tuning is affected by stimulation geometries that mimic different behavioral contexts. Pyramidal cells of the CLS dramatically shifted their frequency tuning from higher to lower frequencies when stimulation was changed from global to local. A similar effect was observed for E-cells of LS, but in this case, it was based largely on increased responses to global high-frequency stimulation without significant changes to mutual information at low AM frequencies.

UPPER-BOUND ESTIMATE. To determine whether the results obtained with the lower bound were robust, we also computed an upper-bound estimate on the information tuning curves (Chacron 2006; Marsat and Pollack 2004; Middleton et al. 2006; Passaglia and Troy 2004; Roddey et al. 2000) (Fig. 3, *B* and *D*; see METHODS).

Similar to the lower-bound estimate, the frequencies at which the upper-bound estimates of E-cell information tuning curves were maximal increased from medial to lateral (data not shown). The differences in mean tuning peaks of E-cells were significant between CMS and LS for global stimulation ($P < 0.01$) and between LS and both CMS and CLS for local stimulation ($P < 0.05$). The mean tuning peaks were much more similar for I-cells of the three segments with none of the differences being significant. The statistical comparison of the two stimulation conditions, global, and local, yielded the same result as for the lower bound on mutual information: E-cells of CLS and LS and I-cells of CLS showed a significant shift of their tuning peaks to lower frequencies, when stimulation was switched from global to local (all paired *t*-test: $P < 0.05$).

Taken together, the picture that emerged for the upper bound closely resembled the one observed for the lower bound with E-cells of CLS showing the strongest and most robust tuning shift to higher modulation frequencies when stimulation was switched from local to global geometry with smaller but statistically significant shifts also seen for LS E-cells.

COMPARISON BETWEEN LOWER AND UPPER BOUNDS. Three observations stand out: First, the upper-bound estimate of mutual information was significantly higher than the lower bound estimate for all maps and cell types (compare Fig. 3, *A* and *B* with *C* and, *D*). Second, the difference between the two estimates is much more pronounced for global stimulation than for local stimulation, and, third, I-cells showed significant information at high (~35 Hz) modulation frequencies when the upper bound was considered but practically none when only

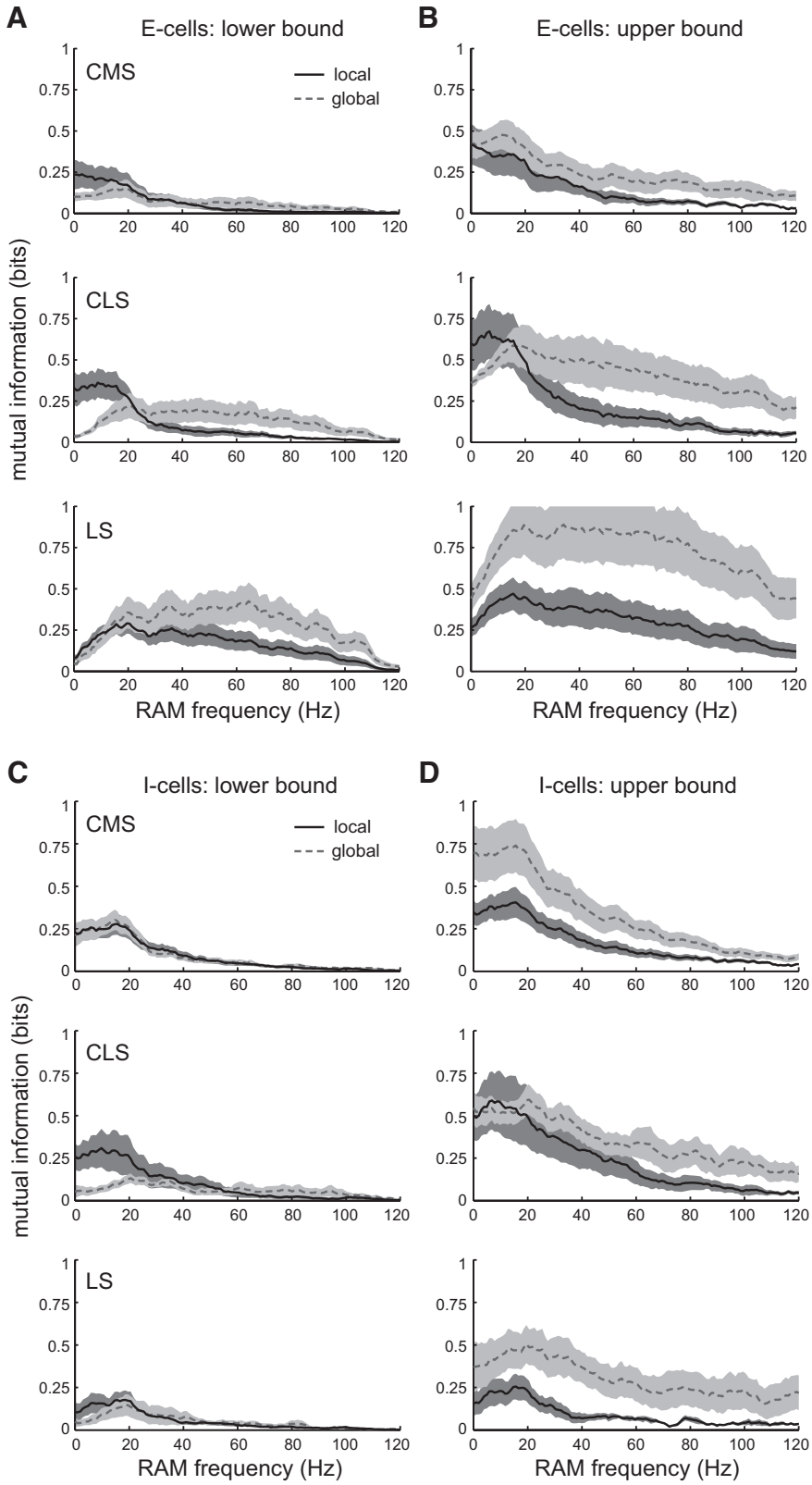

FIG. 3. Population-averaged mutual information tuning curves for global and local stimulation. *A*: average lower bound on mutual information for, from top to bottom, 12 E-cells of CMS, 8 E-cells from CLS, 16 E-cells from LS. *B*: average upper bound on mutual information for, from top to bottom, 12 E-cells of CMS, 8 E-cells from CLS, 16 E-cells from LS. *C*: average lower bound on mutual information for, from top to bottom, 16 I-cells of CMS, 8 I-cells of CLS, 6 I-cells of LS. *D*: average upper bound on mutual information for, from top to bottom, 16 I-cells of CMS, 8 I-cells of CLS, 6 I-cells of LS. —, response to local stimulation; - - -, response to global stimulation; gray areas, SE.

linear information transmission was taken into account. We therefore quantified the difference between the lower and upper bound by computing a performance index, PI, as the ratio of the lower and upper bounds averaged over a given frequency range (see METHODS; see also Chacron (2006). A high value of the PI indicates that most of the information about sensory stimuli could be recovered by a linear decoder; a low value indicates that the majority of the information is transmitted nonlinearly.

When the entire frequency range of RAMs (0–120 Hz) or just the low-frequency range (0–20 Hz) was taken into account, there

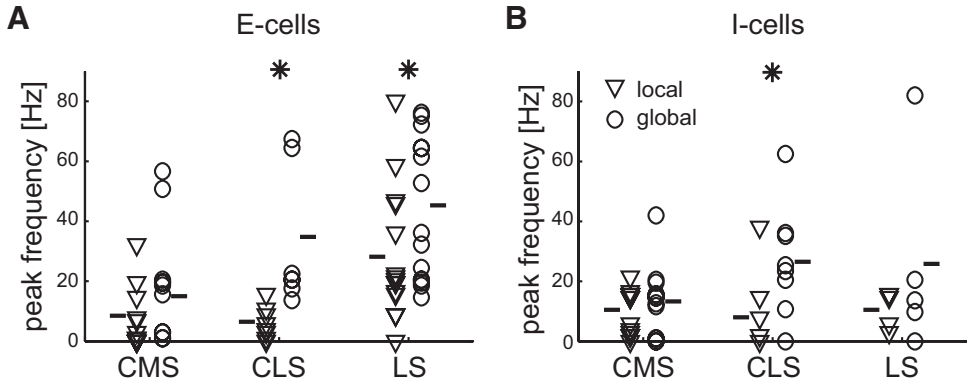

FIG. 4. Comparison of information tuning (lower bound) of pyramidal cells for global and local stimulation. *A* and *B*: peak frequencies of information tuning curves of E-cells (*A*) and I-cells (*B*). Sample sizes: CMS E: $n = 11$; CMS I: $n = 15$; CLS E: $n = 8$; CLS I: $n = 8$; LS E: $n = 15$; LS I: $n = 5$. Triangles, local stimulation; circles, global stimulation. Mean values are indicated by horizontal bars. Asterisks indicate statistically significant differences (paired *t*-test, $P < 0.05$).

was no statistically significant difference in either PI_{0-120} or PI_{0-20} across maps for E-cells (Fig. 5, *A* and *C*). There was, however, a slight trend for PI_{0-120} to increase from CMS over to CLS and LS. This was confirmed for the high-frequency range (PI_{80-100}) for which we found significant differences across maps for local stimulation with the pairwise difference between CMS and LS being significant ($P < 0.05$; Fig. 5*E*). For I-cells, no significant differences between maps in PI were observed for any frequency range (Fig. 5, *B*, *D* and *F*).

However, changing the stimulation geometry from local to global caused clear increases in PI that were statistically significant except for CLS pyramidal cells (Fig. 5, *A* and *B*; Table 2).

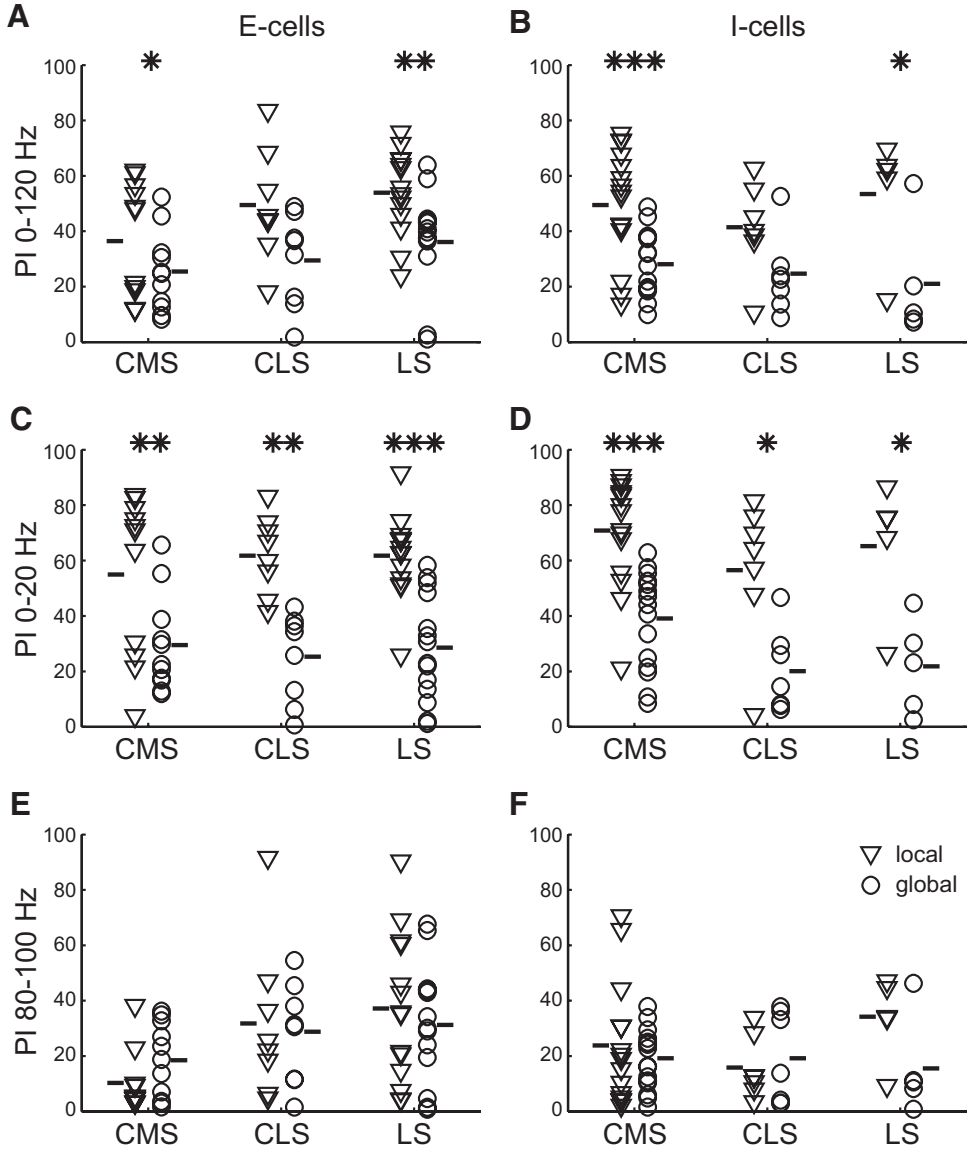

FIG. 5. Percentage of information that can be decoded linearly for E- and I-cells of the 3 maps. The performance index was calculated over the entire frequency range of stimulation ($PI_{0\text{-}120Hz}$) for E-cells (*A*) and I-cells (*B*), for the low-frequency range ($PI_{0\text{-}20Hz}$) for E-cells (*C*) and I-cells (*D*), and for the high-frequency range ($PI_{80\text{-}100Hz}$) for E-cells (*E*) and I-cells (*F*). Triangles, local stimulation; circles, global stimulation. Mean values are indicated by horizontal bars. The asterisks indicate the level of statistical significance for the comparison of local and global performance indices (paired *t*-test): 1 asterisk: $P < 0.05$; 2 asterisks: $P < 0.01$; 3 asterisks: $P < 0.001$.

TABLE 2. *Statistical comparison of performance indices*

	$PI_{0–120Hz}$ Global vs. Local	$PI_{0–20Hz}$ Global vs. Local	$PI_{80–100Hz}$ Global vs. Local	$PI_{0–20Hz}$ vs. $PI_{80–100Hz}$ Global	$PI_{0–20Hz}$ vs. $PI_{80–100Hz}$ Local
CMS E (11)	0.018*	0.009**	0.058	0.014*	0.0002***
CLS E (8)	0.1	0.01*	0.780	0.603	0.007**
LS E (14)	0.006**	0.00006***	0.469	0.631	0.016*
CMS I (15)	0.0002***	0.0006***	0.453	0.0005***	0.00001***
CLS I (7)	0.157	0.061	0.866	0.777	0.005**
LS I (5)	0.031*	0.021	0.148	0.432	0.006**

Values in parentheses indicate sample sizes. Statistical comparison of performance indices for global and local stimulation and of performance indices for a low- and a high-frequency range ($PI_{0–20Hz}$ and $PI_{80–100Hz}$). Shown are P values resulting from paired t-tests. *, $P < 0.05$; **, $P < 0.01$; ***, $P < 0.001$.

This difference turned out to be carried entirely by differences in PI at low stimulus frequencies (Fig. 5, *C* and *D*; Table 2) because at high frequencies, we did not find any differences in PI between local and global stimulation geometries (Fig. 5, *E* and *F*; Table 2). Local responses to low frequencies were significantly more linear than the responses to high frequencies ($PI_{0–20} > PI_{80–100}$; compare Fig. 5, *C* with *E* and *D* with *F*; Table 2). For global stimulation, only E- and I-cells of CMS showed significantly lower performance indices at high frequencies. These results underline our finding that, even though information as measured by the lower bound can be small for I-cells at high frequencies (Fig. 3), the information as measured by the upper bound can be significant.

TOTAL INFORMATION. The information tuning curves of Fig. 3 also suggest differences between the cell types in how much information they encode. We therefore quantified the total amount of mutual information by integrating over the entire stimulus frequency range from 0 to 120 Hz (Fig. 6). The general pattern was the same for the lower- and for the upper-bound estimates (compare Fig. 6, *A* with *C* and *B* with *D*). In both cases, we observed a significant increase in the total amount of information from CMS to CLS to LS for E-cells when they were stimulated globally with the pairwise comparisons being significant for CMS and LS ($P < 0.05$). The increase was less pronounced and not significant for local stimulation. For I-cells, an opposite trend (decrease from CMS to CLS to LS) was apparent but not significant (ANOVA: $P > 0.1$ in all cases).

Responses to naturalistic sinusoidal stimuli

Because natural communication stimuli of *A. leptorhynchus* consist of periodic, quasi-sinusoidal, amplitude modulations that can reach frequencies of >100 Hz (Zakon et al. 2002), we decided to quantify the responses to SAMs between 5 and 125 Hz by calculating the vector strength.

The vector-strength tuning curves had qualitatively the same shape as both lower and upper-bound information-tuning curves (compare Figs. 3 and 7). Vector-strength tuning of E-cells of all maps showed some dependence on stimulus geometry with significantly higher peak frequencies for global stimulation (paired t-test: $P < 0.01$ in all 3 maps). The strongest effects were observed in E-cells of

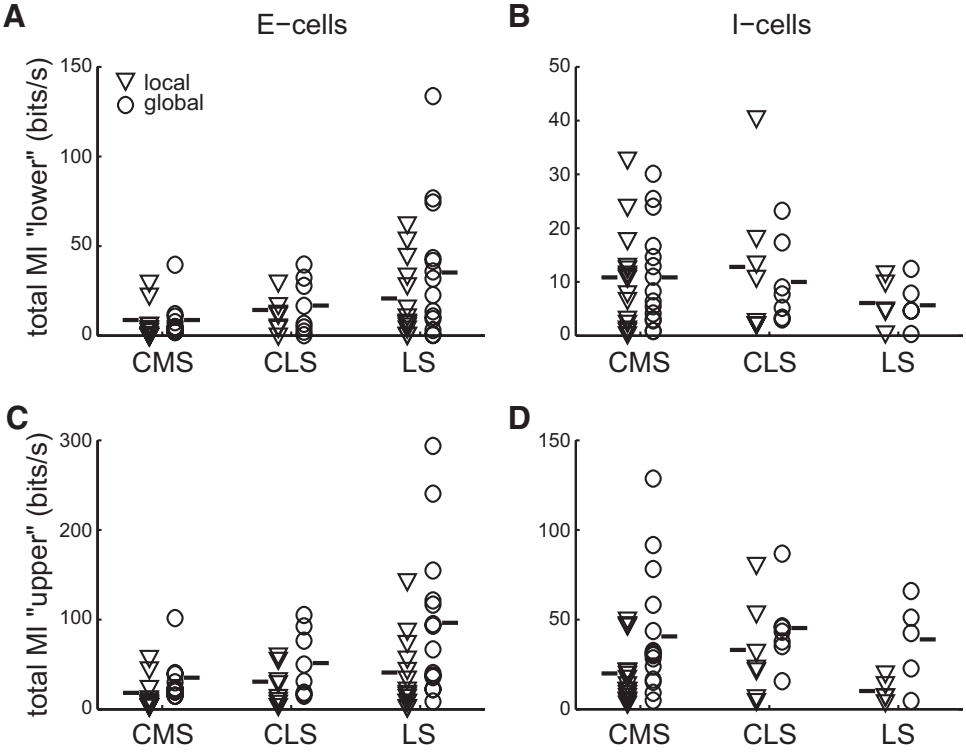

FIG. 6. Total mutual information over the entire frequency range of stimulation (0–120 Hz) for E-cells (*A* and *C*) and I-cells (*B* and *D*). *A* and *B*: lower bound on mutual information. *C* and *D*: upper bound on mutual information. Triangles: local stimulation. Circles, global stimulation. Some values are hidden, because they were plotted on top of each other. Mean values are indicated by horizontal bars.

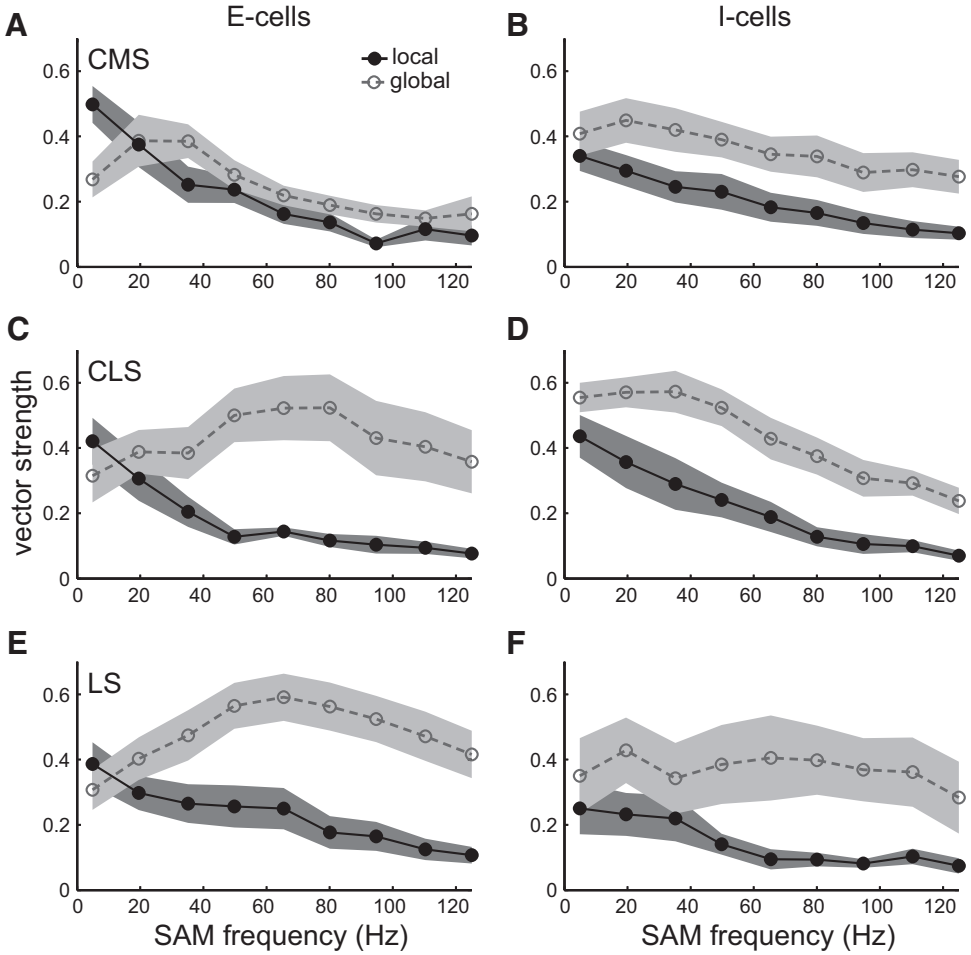

FIG. 7. Frequency tuning of phase locking of pyramidal cell responses to sinusoidal amplitude modulations (SAMs). Population data for vector strength are shown for *A*: CMS E-cells, $n = 11$; *B*: CMS I-cells, $n = 16$; *C*: CLS E-cells, $n = 8$; *D*: CLS I-cells, $n = 9$; *E*: LS E-cells, $n = 15$; *F*: LS I-cells, $n = 5$. —, response to local stimulation; - - -, response to global stimulation; gray areas, ±1 SE.

CLS and only slightly weaker effects in E-cells of LS. These neurons phase-locked most strongly to global stimulation in the range between 40 and 100 Hz and to local stimulation <20 Hz (Fig. 7, *C* and *E*) (see also Chacron et al. 2003). Most surprisingly, LS E-cells showed a low-pass characteristic for local SAM stimulation in contrast to the corresponding information tuning curves (Fig. 3, *A* and *B*), indicating possible interactions among different frequencies characteristic of nonlinear systems.

I-cells of all maps displayed less sharp frequency tuning than E-cells and responded with low- or all-pass filtering for both stimulus geometries. Only I-cells of CLS displayed significantly higher tuning peak frequencies for global than for local geometry ($P < 0.05$). Most strikingly, we found significant phase locking of I-cells even at high frequencies (>40 Hz) where the lower-bound estimate indicated extremely poor information transmission (Fig. 3*C*). Therefore it seems likely that the simultaneous presentation of high- and low-frequency amplitude modulations in RAMs weakens the ability of pyramidal cells to linearly encode information about high stimulus frequencies.

We conclude that similar to our results obtained with RAMs, CLS cells showed the most pronounced shift in tuning as quantified by vector strength when stimulation was switched from global to local with LS E-cells showing similar and also highly significant changes. Furthermore the switch in frequency tuning is more pronounced in E-cells than in I-cells.

Adaptation to step stimuli

The frequency filtering properties of neurons have been linked to how strongly these cells adapt to step changes in their input (Bastian and Courtright 1991; Benda and Herz 2003; Benda et al. 2005), the presence of Ca^{2+}-dependent K^+ channels (Ellis et al. 2007; Wang 1998), and the density of certain interneuron types in the molecular layer of the ELL (Maler and Mugnaini 1994; Shumway 1989b). We therefore subjected pyramidal cells of the different maps to step changes in amplitude and investigated the adaptation properties of their responses by computing the peristimulus time histogram (PSTH).

The responses of E-cells in all three maps to step increases in global EOD amplitude were characterized by a strong transient increase in firing rate that quickly returned to baseline activity levels (Fig. 8). Step increases in local EOD amplitude, in contrast, caused more tonic activity with much slower adaptation. We determined the adaptation time constant, τ, from an exponential fit to the decreasing part of each neuron's PSTH (Fig. 9). For global stimulation, E-cells of CMS had significantly longer time constants than E-cells of both CLS and LS ($P < 0.001$), a finding that matches the frequency tuning properties observed with global RAM and SAM stimulation. For local stimulation, the time constants of CMS and CLS E-cells were statistically indistinguishable, and both were significantly longer that the time constants of LS E-cells ($P < 0.001$), again consistent with the frequency tuning properties

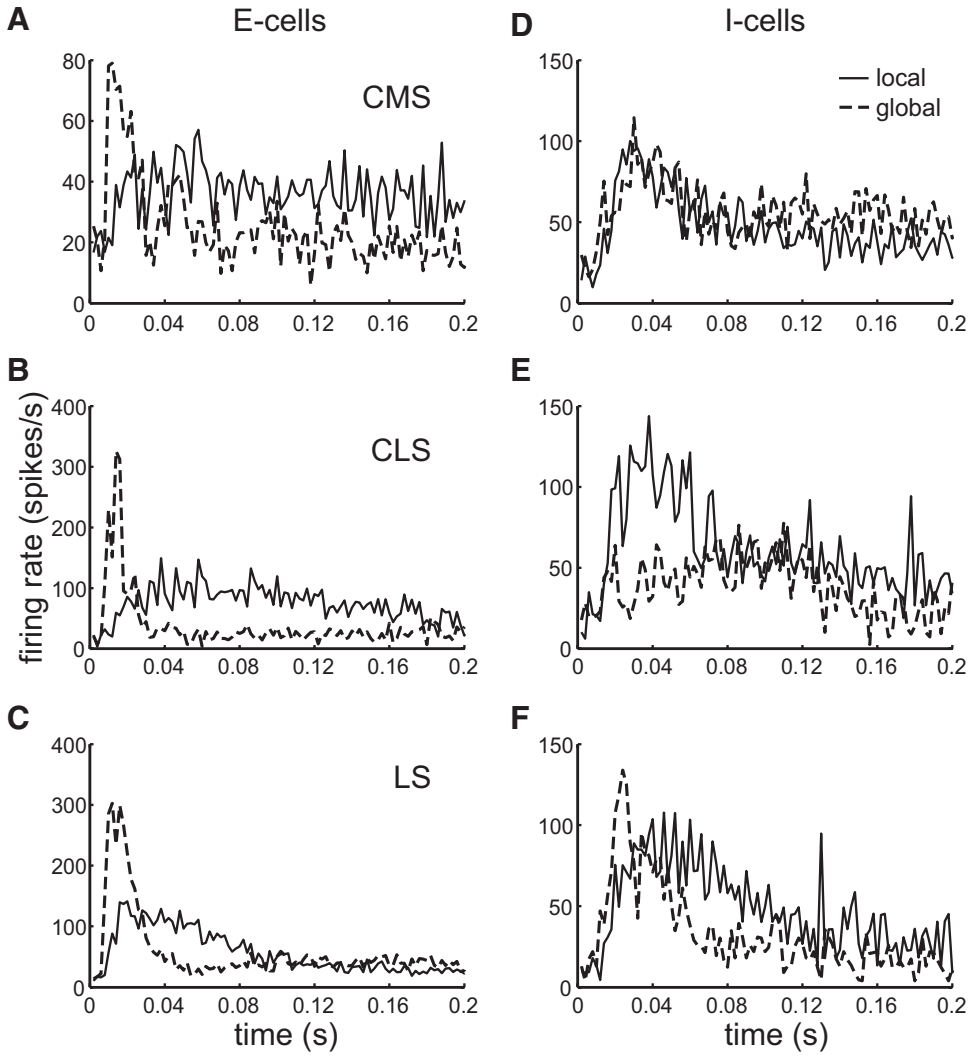

FIG. 8. Mean responses of E-cells to step increases in amplitude and of I-cells to step decreases in amplitude (duration of steps: 200 ms). *A*: E-cells of CMS. $n = 8$. *B*: I-cells of CMS. $n = 7$. *C*: E-cells of CLS. $n = 3$. *D*: I-cells of CLS. $n = 5$. *E*: E-cells of LS. $n = 10$. *F*: I-cells of LS. $n = 3$. - - -, response to global stimulation; —, response to local stimulation.

observed with local RAM and SAM stimulation. The adaptation time constants of E-cells of all maps under global stimulation were significantly shorter than those measured under local stimulation (paired *t*-test: $P < 0.01$). The time constants of CMS E-cells varied enormously under local stimulation; this was largely due to the poor local responses of some of these cells.

The responses of I-cells were overall more tonic than those of E-cells and did not differ significantly in their adaptation time constants under global or under local stimulation (ANOVA for both global and local: $P > 0.5$).

Contribution of Ca^{2+}-dependent processing to frequency tuning

Previous studies have demonstrated segmental differences in Ca^{2+}-associated proteins; both ryanodine receptors (Zupanc et al. 1992) and SK channels (Ellis et al. 2007) are relatively enriched in LS in comparison to CMS. Furthermore in vitro studies have shown that LS E-cells showed high-pass frequency tuning to noise current injections, while CMS E-cells were more low-pass (Ellis et al. 2007). This raises the interesting possibility that the differences in tuning seen in vivo are due to intrinsic rather than

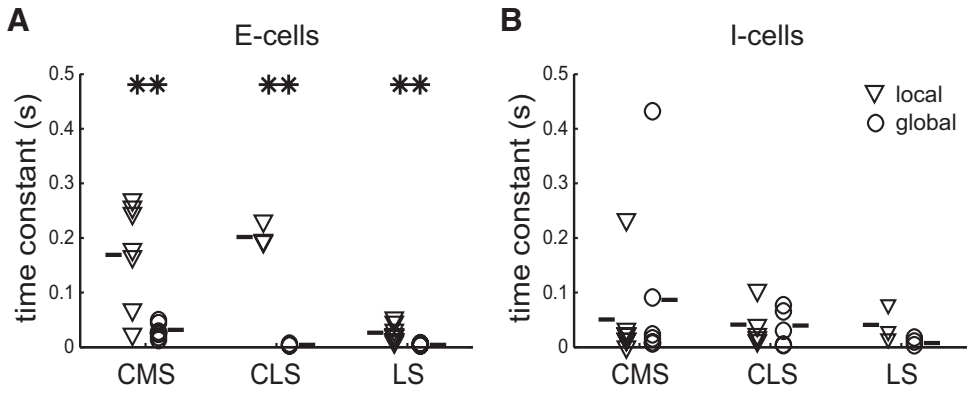

FIG. 9. Adaptation time constants of the responses of pyramidal cells as determined from the step responses shown in Fig. 8. *A* and *B*: median adaptation time constants of E-cells (*A*) and I-cells (*B*). Triangles, local stimulation; circles, global stimulation. Some values are hidden because they were plotted on top of each other. Mean values are indicated by horizontal bars. Two asterisks in *A* indicate that the time constants of E-cells in response to local step stimuli were significantly larger than for global step stimuli (paired *t*-test, $P < 0.01$).

network level mechanisms. We therefore used the Ca^{2+} chelator BAPTA to explore the potential role of Ca^{2+}-activated processes in frequency tuning of pyramidal cells. We recorded intracellularly from 28 pyramidal cells with sharp electrodes filled with BAPTA (see METHODS). To avoid effects of passive leakage of BAPTA from the electrode during the control recordings, we limited the stimulation protocol to global RAM stimulation.

The information tuning curves measured intracellularly in CMS and CLS/LS under control conditions, with global stimulation, corresponded well to the ones measured with extracellular electrodes (compare control curves in Fig. 10, *A* and *B* with Fig. 3). CMS cells displayed low-pass filtering, whereas CLS/LS cells showed high-pass/band-pass behavior. Following iontophoretic injection of BAPTA, information tuning remained virtually unchanged in CMS cells (Fig. 10*A*). In the CLS/LS, tuning shifted to lower frequencies; this was due to a dramatic decrease of high-frequency tuning as well as a smaller increase in tuning to frequencies <20 Hz (Fig. 10*B*). This change could be quantified as a significant shift in tuning peaks of CLS/LS neurons to lower frequencies (Fig. 10*C*; from 56.2 ± 27.3 to 29.1 ± 15.8 Hz following BAPTA application; paired *t*-test: $P < 0.01$; $n = 14$). This finding shows that Ca^{2+}-dependent processes are involved in shaping frequency tuning of pyramidal cells of the two more lateral maps and contribute to the differential tuning of pyramidal cells to local versus global stimuli within each map. In CMS, Ca^{2+}-dependent processes are either less prevalent and/or they do not affect frequency tuning of pyramidal cells. This is consistent with previous studies showing a lower density, in CMS compared with LS, of both *N*-methyl-D-aspartate (NMDA) receptors (Harvey-Girard et al. 2007) and Ca^{2+}-activated K^+ channels (Ellis et al. 2007). Our results are furthermore consistent with those of Ellis et al. (2007), who showed that small conductance Ca^{2+}-activated K^+ channels had a strong effect on the frequency tuning of pyramidal cells (but see DISCUSSION).

Modeling Ca^{2+}-dependent processes in pyramidal cells

To determine whether blockade of Ca^{2+}-activated K^+ channels by BAPTA could explain the changes in the information tuning seen in CLS/LS, we built a pyramidal cell model incorporating Ca^{2+}-activated K^+ currents. Our results show that the presence of Ca^{2+}-activated K^+ currents can have a significant effect on information transmission (Fig. 11*A*). Such currents can give rise to weaker responses at low frequencies and stronger responses at high frequencies, thereby shifting the frequency at which the response is maximal in a manner reminiscent of our BAPTA experiments (compare with Fig. 10*B*). Consistent with previous reports (Connors et al. 1982; Liu and Wang 2001; Wang 1998), inspection of spike shape revealed a more pronounced afterhyperpolarization (AHP) with Ca^{2+}-activated K^+ currents present (Fig. 11*B*).

Our model predicted that the main effect of BAPTA was to inhibit the activation of Ca^{2+}-activated K^+ channels, thereby reducing the AHP and thus shifting the frequency tuning of pyramidal cells. Therefore our model predicts that BAPTA should reduce the AHP in CLS/LS pyramidal cells and have no effect on the AHP of CMS cells. Consistent with this prediction, we observed experimentally that BAPTA injection significantly reduced the AHP in CLS/LS cells (average: 2.31 ± 1.03 mV, $P = 0.002$, pairwise *t*-test, $n = 6$; Fig. 11*C*), whereas BAPTA had virtually no effect on the AHP in CMS recordings (0.1 ± 0.24 mV, $P = 0.55$, pairwise *t*-test, $n = 7$). Thus Ca^{2+}-activated K^+ currents are most likely partly responsible for the differences in frequency tuning observed with BAPTA and more generally those seen across ELL segments.

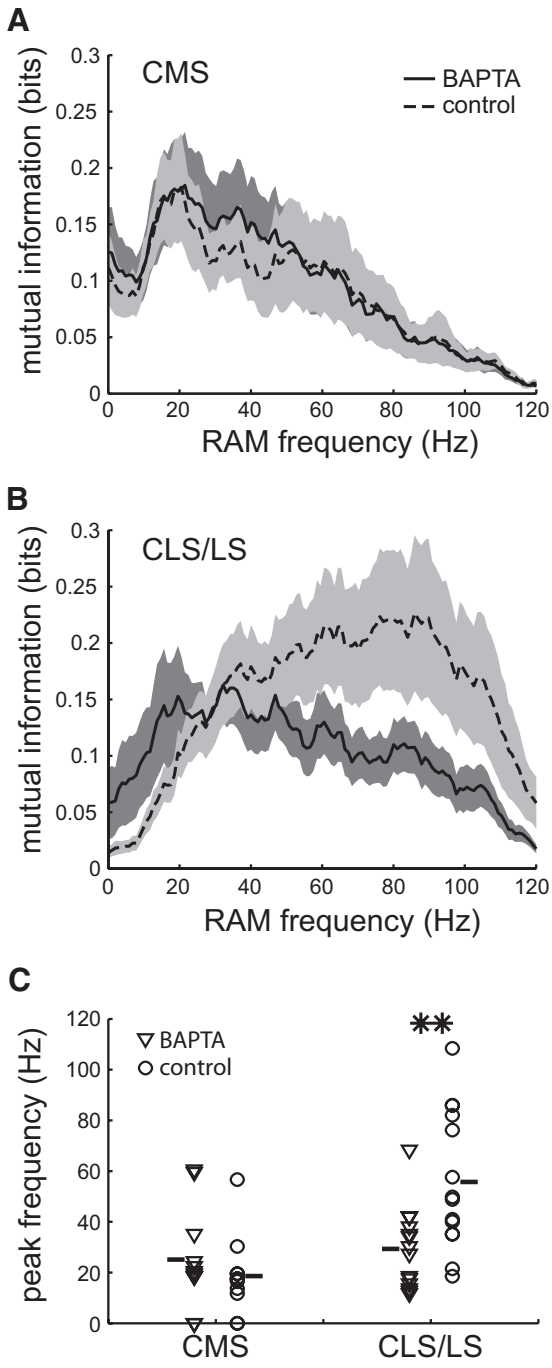

FIG. 10. Effect of blocking intracellular Ca^{2+} on information tuning of pyramidal cells. Population averages of mutual information measured in pyramidal cells in CMS (*A*) ($n = 14$ cells) and CLS/LS (*B*) ($n = 15$ cells). *C*: peak frequencies of information tuning curves of pyramidal cells in CMS and CLS/LS under control conditions (circles) and following iontophoretic injection of BAPTA (triangles). Mean values in *C* are indicated by horizontal bars. The 2 asterisks indicate that the peak frequencies after bis-(*o*-aminophenoxy)-*N,N,N′,N′*-tetraacetic acid (BAPTA) application were significantly lower than under control conditions (paired *t*-test, $P < 0.01$).

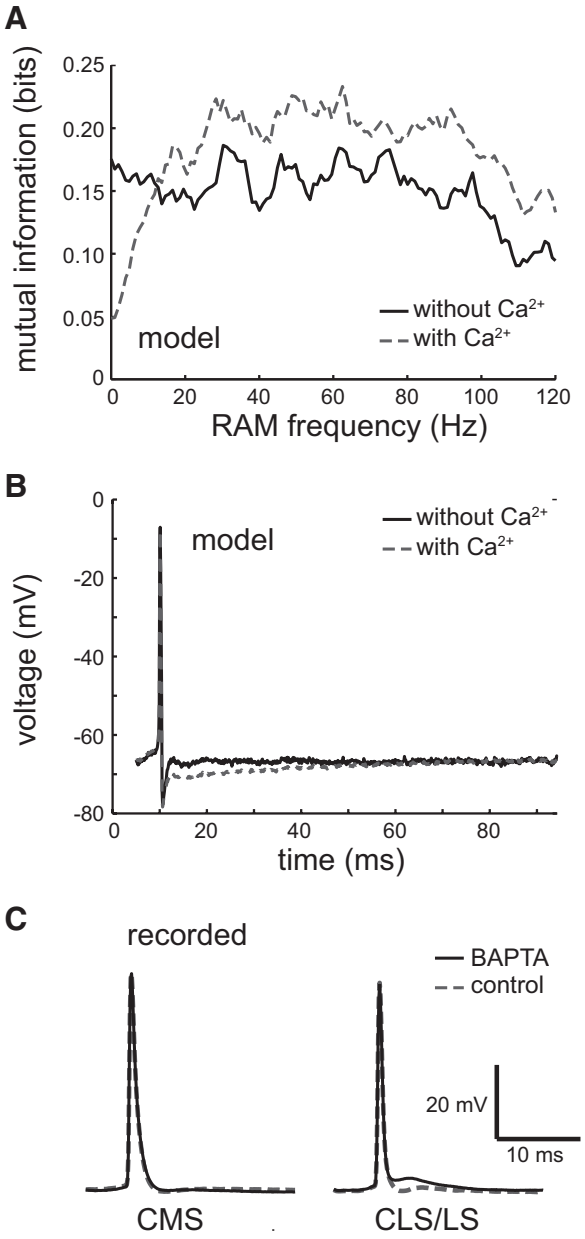

FIG. 11. Modeling the effect of Ca^{2+}-dependent K^+ currents on information transmission. *A*: mutual information density curves obtained with (dashed gray line) and without (solid black line) a Ca^{2+}-activated K^+ channel. *B*: spike shapes with (dashed gray line) and without (solid black line) a Ca^{2+}-activated K^+ channel. *C*: spike shapes before (dashed gray line) and after (solid black line) BAPTA iontophoresis for a pyramidal cell recorded in CMS (*left*) and a cell recorded in CLS/LS.

DISCUSSION

Summary of results

The present study provides the first comparison of frequency tuning across cell types and segments of the ELL of weakly electric fish for two different behaviorally relevant stimulus conditions: local stimulation that mimics the effects of electrolocation input (e.g., prey) versus global stimulation that occurs during interactions with conspecifics. Our results showed no significant differences in the baseline activity across the segments save for a higher phase locking to the animal's EOD for LS E-cells. We found, however, an unexpected difference between the segments under driven conditions: cells within the CLS segment showed the most dramatic switch in frequency tuning contingent on stimulation geometry (Chacron 2006; Chacron et al. 2003, 2005b) followed by LS E-cells, whereas cells within the CMS showed tuning that was largely independent of the stimulus' spatial extent for all stimuli used within this study: E-cells of CMS acted as low-pass filters under both geometries. E-cells of CLS acted as low-pass filters for local and as high-pass/band-pass filters for global geometry. For E-cells of LS, their response characteristics depended most obviously on the type of stimulus used: RAM or SAM stimulation. Under SAM stimulation, these cells displayed a switch in tuning similar to CLS E-cells, whereas under RAM stimulation, they increased their high-frequency responsiveness when driven globally and responded poorly to low frequencies under both conditions. I-cells of all maps can be described as low-pass filters under both stimulus conditions with CMS and LS I-cells displaying tuning that was independent of the stimulation geometry.

Finally, our results show that differences in tuning across the segments are in large part mediated by intrinsic Ca^{2+}-dependent mechanisms rather than network level mechanisms. This is consistent with the distributions of both NMDA receptors (Harvey-Girard et al. 2007) and Ca^{2+}-activated K^+ channels (Ellis et al. 2007). Further support for intrinsic cellular properties being a major factor for frequency tuning comes from a recent in vitro study of ELL pyramidal cells (Mehaffey et al. 2008).

Our information-theoretic analysis (Figs. 3, 5, 7) indicates that a significant fraction of the information about sensory stimuli must be recovered by a nonlinear decoder (Chacron 2006; Marsat and Pollack 2004; Passaglia and Troy 2004). We observed that linear decoders could recover a greater fraction of the total information for local as compared with global stimulation as quantified by the performance index confirming earlier results (Chacron 2006). This difference was due largely to the responses to low AM frequencies. At higher AM frequencies, we found no significant differences in PI between stimulation geometries. Most interestingly, low-pass neurons (CMS cells and all I-cells) displayed significant information at high frequencies that could not be recovered by a linear decoder. This was verified by the strong responses to high-frequency sinusoidal AMs. Thus nonlinear interactions between frequencies can be expected to shape pyramidal cell responses in situations when multiple frequencies are present simultaneously as occurs, for example, during encounters with several conspecifics (Tan et al. 2005) and when communication signals interfere with local signals arising from prey or environmental objects. Nonlinear interactions between frequencies may also be the reason why LS E-cells showed band-pass behavior for local RAM stimulation and low-pass behavior when local SAMs were presented. We conclude that linear measures of stimulus-response characteristics, such as the lower bound on the information tuning curve, may severely underestimate the ability of sensory neurons to convey information about behaviorally relevant stimuli.

Differences in frequency tuning across ELL segments and relation to behavior

The three segments of the ELL receive identical input from the primary electrosensory afferents (Heiligenberg and Dye 1982).

The frequency response of the receptor afferents is broadband when measured as information tuning curves (Chacron et al. 2005a,b), and pyramidal cells appear to select different frequency ranges from this input depending on the cell type and segment of the ELL. The observed differences in frequency tuning for global stimuli correlate well with proposed functional roles for each map in different behaviors. Metzner and Juranek (1997) showed that the CMS is necessary and sufficient for a certain electric behavior, the jamming avoidance response (JAR) (see Heiligenberg 1991), while the LS is necessary and sufficient for a communication response called chirping. The JAR is elicited only by low-frequency global signals that arise when a nearby conspecific has a similar EOD frequency as the focal fish. This is consistent with Shumway's (1989a) and our finding that CMS is the only map that responds preferentially to global low-frequency stimuli. In contrast, chirps are global electrommunication signals that contain high frequencies (Zupanc and Maler 1993) and that are elicited during aggressive and mating behaviors (Engler and Zupanc 2001; Hagedorn and Heiligenberg 1985; Zupanc et al. 2006). High-frequency, global signals would then only be encoded by CLS and LS neurons but not by CMS neurons.

Pyramidal cells must also relay information about the presence and spatial location of prey and other objects in the environment. Relatively distant objects cast weak, diffuse, and spatially extended "electric images" on the skin of the fish. As the distance decreases, the image becomes stronger and smaller (Assad et al. 1999; Babineau et al. 2006; Bastian 1981a; Chen et al. 2005; Nelson and MacIver 1999). Lewis and Maler (2001) proposed a population coding scheme for the determination of object distance that relies on two topographic maps, one with small and one with large receptive fields. The map with small receptive fields would provide reliable information on the width of the electric image of an object on the skin, whereas the map with the large receptive fields would provide reliable information on the peak amplitude of the electric image. Combining these two pieces would allow the determination of object distance (Lewis and Maler 2001). Pyramidal cells of all three maps showed low-pass filtering for local stimulation with SAMs, appropriate for the processing of prey-like stimuli (Nelson and MacIver 1999). It is currently unknown how the receptive field sizes of pyramidal cells differ between maps in *A. leptorhynchus* although they have been measured in great detail for cells of CLS and LS combined (Bastian et al. 2002). A study in the related gymnotiform fish, *Eigenmannia spec.*, however, described the receptive field sizes of CMS cells as small, the ones of CLS as intermediate, and the ones of LS as large (Shumway 1989a). If similar differences in receptive field size exist in *A. leptorhynchus*, CMS would be the map best suited for providing information on the width of electric images of objects, and CLS and LS would be well suited to carry information on image amplitude with CLS being best for small to intermediate distances and LS best for the largest distances, at which electric images are widest (Assad et al. 1999; Babineau et al. 2006; Bastian 1981a; Chen et al. 2005; Nelson and MacIver 1999). Additional support for this interpretation comes from Shumway (1989a)'s finding that LS pyramidal cells had the lowest thresholds for amplitude modulations. The assumption of large receptive fields for LS (larger convergence of primary afferents) is also consistent with our finding that LS E-cells showed the strongest phase coupling to the EOD and had the highest values of total mutual information among E-cells.

Multiple maps occur in a range of sensory systems, such as the visual, auditory, and somatosensory system (Catania 2002; MacLeod and Carr 2007; Van Essen and Gallant 1994; Wässle 2004). Electrosensory systems may offer particular insight into the evolution of multiple maps. Several groups of fish, teleost and nonteleost, possess an ampullary electrosensory system dedicated to processing the low-frequency electric fields generated by the bodies of prey (Bell and Maler 2005). These ampullary systems all rely on a single topographic map in the hindbrain. Two groups of teleost fish, the African mormyriforms and the South-American gymnotiforms, independently evolved electrogeneration and an electrosensory system dedicated to processing perturbations of the self-generated electric field. These tuberous electrosensory systems appear to be derived from the ancestral ampullary system. Interestingly, in each group, the tuberous system evolved multiple representations of the electroreceptive body surface (Bell and Maler 2005), suggesting a more dominant role for sensory information acquisition of the tuberous compared with the ampullary systems. In view of the complex specialization of cortical visual maps (Van Essen and Gallant 1994), the differences between the three tuberous maps described here and by Shumway (1989a,b) appear relatively small even though they seem to be essential for the observed complexity of electrosensory behaviors (Metzner 1999). The following, certainly speculative, picture for the evolution of these maps emerges: CLS may be the evolutionarily oldest segment in this system with the ability to switch frequency selectivity according to the processing demands of prey or communication stimuli. CMS and LS may have arisen later in one or two map-multiplication steps and then evolved to specialize on processing certain subsets of relevant stimuli: signals of nearby prey and low-frequency communication signals in the context of the JAR in the case of CMS and signals of distant prey and higher-frequency communication signals in the case of LS.

Cellular mechanisms contributing to observed differences in frequency tuning across segments

The Ca^{2+} chelator BAPTA had a significant effect on the information tuning curves of CLS/LS cells but not CMS cells. As shown by our model, Ca^{2+}-activated K^+ channels could account for the effect of BAPTA. The model predicted that BAPTA should reduce the AHP following each spike in CLS/LS but not in CMS, which was supported by our experimental observations. It therefore appears that it is primarily intrinsic cellular mechanisms that are responsible for differences in tuning across the segments rather than network interactions. This is supported by recent in vitro studies showing differences in tuning to noise current injections that are similar to those seen here for E and I-cells and across segments (Ellis et al. 2007; Mehaffey et al. 2008). A likely candidate mechanism for observed tuning differences is the graded expression of SK channels (Ellis et al. 2007). The strongest expression was found in LS and the weakest in CMS (Ellis et al. 2008). Whereas SK1 channels were found in dendrites of both E- and I-cells, SK2 channels were primarily found in E-cell somata as supported by apamin blocks in the pyramidal cell layer (Ellis et al. 2007, 2008). As Ca^{2+}-activated K^+ channels have been

shown to contribute to increased responses to high frequencies at the expense of decreased responses to low frequencies (Benda and Herz 2003; Benda et al. 2005; Connors et al. 1982; Liu and Wang 2001; Wang 1998), the expression of both SK1 and SK2 channels is consistent with the differential tuning properties observed both in vitro and in vivo across segments as well as between E- and I-cells.

Previous pharmacological studies have shown that different SK channel subtypes had differential affinity for apamin: SK2 having the highest while SK1 having the lowest (Nolting et al. 2007). Current pharmacological techniques (Bastian 1993; Bastian et al. 2004; Chacron 2006; Chacron and Bastian 2008; Chacron et al. 2005b) are designed to deliver pharmacological agents to the dorsal molecular layer of the ELL. Previous studies have shown that these agents did not diffuse past the tractus stratum fibrosum (Bastian 1993), which forms a boundary between the pyramidal cell layer and the molecular layer containing the apical dendrites of pyramidal cells. This boundary is one likely reason for the lack of effect of apamin when ejected into the molecular layer (see METHODS): it probably did not reach the pyramidal cell somata where SK2 channels are found (Ellis et al. 2007, 2008). In principle, apamin could still have had an effect on pyramidal cells via the dendritic SK1 channels. It is possible that the lack of effect is due to the low affinity of SK1 channels for apamin. This is furthermore consistent with the lack of effect of apamin seen on I-cells in vitro (Ellis et al. 2007). A complete characterization of the role played by SK channels in determining the frequency tuning of pyramidal cells in vivo is beyond the scope of this paper.

Alternatively, other Ca^{2+}-dependent currents may be involved in the observed effects of BAPTA on frequency tuning in the ELL as well. Apamin-insensitive Ca^{2+}-activated currents that give rise to a slow AHP have been described in several other systems (Faber and Sah 2002; Hirst et al. 1985; Lancaster and Nicoll 1987) and have been shown to mediate spike frequency adaptation (Faber and Sah 2003). An apamin-insensitive slow AHP has been observed in LS and CLS cells in vitro (L. Ellis, personal communication). Furthermore, while apamin enhanced low-frequency tuning of CLS and LS E cells, it had little effect on their response to high-frequency input (Ellis et al. 2007). This is in contrast to our results that showed a very strong reduction of the CLS/LS cells' high-frequency response after BAPTA treatment (Fig. 10). This suggests that BAPTA blocks an additional apamin-insensitive Ca^{2+}-dependent K^+ channel of CLS/LS cells (high-frequency effect of BAPTA) as well as the SK channel (low-frequency effect of BAPTA and apamin). It is possible that this additional channel is, in fact, the one that causes the slow AHP observed by Ellis (personal communication) Additional studies are needed to determine the contribution of such currents to frequency tuning in the ELL. However, to our knowledge, there are currently no known specific blockers for the slow AHP.

ACKNOWLEDGMENTS

We are grateful to two anonymous reviewers for helpful comments.

GRANTS

The research presented in this article was supported by National Institute of Neurological Disorders and Stroke Grant NS-12337 to J. Bastian, National Sciences and Engineering Research Council funding to R. Krahe, and Canadian Institute of Health Resources funding to M. J. Chacron.

REFERENCES

Abeles M. Quantification, smoothing, and confidence limits for single units' histograms. *J Neurosci Methods* 5: 317–325, 1982.

Assad C, Rasnow B, Stoddard PK. The electric organ discharges and electric images during electrolocation. *J Exp Biol* 202: 1185–1193, 1999.

Babineau D, Longtin A, Lewis JE. Modeling the electric field of weakly electric fish. *J Exp Biol* 209: 3636–3651, 2006.

Bastian J. Electrosensory input to the corpus cerebelli of the high-frequency electric fish *Eigenmannia virescens. J Comp Physiol* 90: 1–24, 1974.

Bastian J. Electrolocation. I. How the electroreceptors of *Apteronotus albifrons* code for moving objects and other electrical stimuli. *J Comp Physiol [A]* 144: 465–479, 1981a.

Bastian J. Electrolocation. II. The effects of moving objects and other electrical stimuli on the activities of two categories of posterior lateral line lobe cells in *Apteronotus albifrons. J Comp Physiol [A]* 144: 481–494, 1981b.

Bastian J. The role of amino-acid neurotransmitters in the descending control of electroreception. *J Comp Physiol [A]* 172: 409–423, 1993.

Bastian J. Modulation of calcium-dependent postsynaptic depression contributes to an adaptive sensory filter. *J Neurophysiol* 80: 3352–3355, 1998.

Bastian J, Chacron MJ, Maler L. Receptive field organization determines pyramidal cell stimulus-encoding capability and spatial stimulus selectivity. *J Neurosci* 22: 4577–4590, 2002.

Bastian J, Chacron MJ, Maler L. Plastic and nonplastic pyramidal cells perform unique roles in a network capable of adaptive redundancy reduction. *Neuron* 41: 767–779, 2004.

Bastian J, Courtright J. Morphological correlates of pyramidal cell adaptation rate in the electrosensory lateral line lobe of weakly electric fish. *J Comp Physiol [A]* 168: 393–407, 1991.

Bastian J, Nguyenkim J. Dendritic modulation of burst-like firing in sensory neurons. *J Neurophysiol* 85: 10–22, 2001.

Bell CC, Maler L. Central neuroanatomy of electrosensory systems in fish. In: *Electroreception*, edited by Bullock TH, Hopkins CD, Popper AN, Fay RR. New York: Springer, 2005, p. 68–111.

Benda J, Herz AVM. A universal model for spike-frequency adaptation. *Neural Comput* 15: 2523–2564, 2003.

Benda J, Longtin A, Maler L. Spike-frequency adaptation separates transient communication signals from background noise oscillations. *J Neurosci* 25: 2312–2321, 2005.

Berman NJ, Maler L. Distal versus proximal inhibitory shaping of feedback excitation in the electrosensory lateral line lobe: implications for sensory filtering. *J Neurophysiol* 80: 3214–3232, 1998a.

Berman NJ, Maler L. Inhibition evoked from primary afferents in the electrosensory lateral line lobe of the weakly electric fish (*Apteronotus leptorhynchus*). *J Neurophysiol* 80: 3173–3196, 1998b.

Berman NJ, Maler L. Neural architecture of the electrosensory lateral line lobe: adaptations for coincidence detection, a sensory searchlight and frequency-dependent adaptive filtering. *J Exp Biol* 202: 1243–1253, 1999.

Borst A, Theunissen FE. Information theory and neural coding. *Nat Neurosci* 2: 947–957, 1999.

Carr CE, Maler L, Sas E. Peripheral organization and central projections of the electrosensory nerves in gymnotiform fish. *J Comp Neurol* 211: 139–153, 1982.

Catania KC. Barrels, stripes, and fingerprints in the brain - implications for theories of cortical organization. *J Neurocytol* 31: 347–358, 2002.

Chacron MJ. Nonlinear information processing in a model sensory system. *J Neurophysiol* 95: 2933–2946, 2006.

Chacron MJ. Electrolocation. *Scholarpedia* 2: 1411, 2007.

Chacron MJ, Bastian J. Population coding by electrosensory neurons. *J Neurophysiol* 99: 1825–1835, 2008.

Chacron MJ, Doiron B, Maler L, Longtin A, Bastian J. Non-classical receptive field mediates switch in a sensory neuron's frequency tuning. *Nature* 423: 77–81, 2003.

Chacron MJ, Maler L, Bastian J. Electroreceptor neuron dynamics shape information transmission. *Nat Neurosci* 8: 673–678, 2005a.

Chacron MJ, Maler L, Bastian J. Feedback and feedforward control of frequency tuning to naturalistic stimuli. *J Neurosci* 25: 5521–5532, 2005b.

Chen L, House JL, Krahe R, Nelson ME. Modeling signal and background components of electrosensory scenes. *J Comp Physiol [A]* 2005.

Connors BW, Gutnick MJ, Prince DA. Electrophysiological properties of neocortical neurons in vitro. *J Neurophysiol* 97: 2744–2757, 1982.

Ellis LD, Maler L, Dunn RJ. Differential distribution of SK channel subtypes in the brain of the weakly electric fish, *Apteronotus leptorhynchus. J Comp Neurol* 507: 1964–1978, 2008.

Ellis LD, Mehaffey WH, Harvey-Girard E, Turner RW, Maler L, Dunn RJ. SK channels provide a novel mechanism for the control of frequency tuning in electrosensory neurons. *J Neurosci* 27: 9491–9502, 2007.

Engler G, Zupanc GKH. Differential production of chirping behavior evoked by electrical stimulation of the weakly electric fish, *Apteronotus leptorhynchus. J Comp Physiol [A]* 187: 747–756, 2001.

Faber ES, Sah P. Physiological role of calcium-activated potassium currents in the rat lateral amygdala. *J Neurosci* 22: 1618–1628, 2002.

Faber ES, Sah P. Calcium-activated potassium channels: multiple contributions to neuronal function. *Neuroscientist* 9: 181–194, 2003.

Fortune ES. The decoding of electrosensory systems. *Curr Opin Neurobiol* 16: 474–480, 2006.

Fortune ES, Rose GJ, Kawasaki M. Encoding and processing biologically relevant temporal information in electrosensory systems. *J Comp Physiol [A]* 192: 625–635, 2006.

Frank K, Becker MC. Microelectrodes for recording and stimulation. In: *Physical Techniques in Biological Research*, edited by Nastuk WL. New York: Academic, 1964, p. 23–84.

Gardiner CW. *Handbook of Stochastic Methods for Physics, Chemistry, and the Natural Sciences.* Berlin: Springer, 2004.

Graziano MSA, Aflalo TN. Rethinking cortical organization: moving away from discrete areas arranged in hierarchies. *Neuroscientist* 13: 138–147, 2007.

Hagedorn M, Heiligenberg W. Court and spark: electric signals in the courtship and mating of gymnotoid electric fish. *Anim Behav* 33: 254–265, 1985.

Harvey-Girard E, Dunn RJ, Maler L. Regulated expression of N-methyl-D-aspartate receptors and associated proteins in teleost electrosensory system and telencephalon. *J Comp Neurol* 505: 644–668, 2007.

Heiligenberg W. *Neural Nets in Electric Fish*. Cambridge, MA: MIT Press, 1991.

Heiligenberg W, Dye J. Labeling of electroreceptive afferents in a gymnotoid fish by intracellular injection of HRP: the mystery of multiple maps. *J Comp Physiol [A]* 148: 287–296, 1982.

Hirst GDS, Johnson SM, Van Helden DF. The slow calcium-dependent potassium current in a myenteric neuron of the guinea-pig ileum. *J Physiol* 361: 315–337, 1985.

Jarvis MR, Mitra PP. Sampling properties of the spectrum and coherency of sequences of action potentials. *Neural Comput* 13: 717–749, 2001.

Kajikawa Y, Hackett TA. Entropy analysis of neuronal spike train synchrony. *J Neurosci Methods* 149: 90–93, 2005.

Kelly M, Babineau D, Longtin A, Lewis JE. Electric field interactions in pairs of electric fish: modeling and mimicking naturalistic inputs. *Biol Cybern* 98: 479–490, 2008.

Koch C. *Biophysics of Computation.* New York: Oxford, 1999.

Krahe R, Gabbiani F. Burst firing in sensory systems. *Nat Rev Neurosci* 5: 13–23, 2004.

Lancaster B, Nicoll RA. Properties of two calcium-activated hyperpolarizations in rat hippocampal neurones. *J Physiol* 389: 187–203, 1987.

Lewis JE, Maler L. Neuronal population codes and the perception of object distance in weakly electric fish. *J Neurosci* 21: 2842–2850, 2001.

Liu YH, Wang X-J. Spike Frequency adaptation of a generalized leaky integrate-and-fire neuron. *J Comput Neurosci* 10: 25–45, 2001.

MacLeod KM, Carr CE. Beyond timing in the auditory brainstem: intensity coding in the avian cochlear nucleus angularis. *Prog Brain Res* 165: 123–133, 2007.

Maler L, Mugnaini E. Correlating gamma-aminobutyric acidergic circuits and sensory function in the electrosensory lateral line lobe of a gymnotiform fish. *J Comp Neurol* 345: 224–252, 1994.

Maler L, Sas EK, Rogers J. The cytology of the posterior lateral line lobe of high-frequency weakly electric fish (Gymnotidae): dendritic differentiation and synaptic specificity in a simple cortex. *J Comp Neurol* 195: 87–139, 1981.

Mardia KV, Jupp PE. *Directional Statistics.* New York: Wiley, 1999.

Marsat G, Pollack GS. Differential temporal coding of rhythmically diverse acoustic signals by a single interneuron. *J Neurophysiol* 92: 939–948, 2004.

Mehaffey WH, Fernandez FR, Rashid AJ, Dunn RJ, Turner RW. Distribution and function of potassium channels in the electrosensory lateral line lobe of weakly electric apteronotid fish. *J Comp Physiol [A]* 192: 637–648, 2006.

Mehaffey WH, Maler L, Turner RW. Intrinsic frequency tuning in ELL pyramidal cells varies across electrosensory maps. *J Neurophysiol* 99: 2641–2655, 2008.

Metzner W. Why are there so many sensory brain maps? *Cell Mol Life Sci* 56: 1–4, 1999.

Metzner W, Juranek J. A sensory brain map for each behavior. *Proc Natl Acad Sci USA* 94: 14798–14803, 1997.

Metzner W, Koch C, Wessel R, Gabbiani F. Feature extraction by burst-like spike patterns in multiple sensory maps. *J Neurosci* 18: 2283–2300, 1998.

Middleton JW, Longtin A, Benda J, Maler L. The cellular basis for parallel neural transmission of a high-frequency stimulus and its low-frequency envelope. *Proc Natl Acad Sci USA* 103: 14596–14601, 2006.

Nelson ME, MacIver MA. Prey capture in the weakly electric fish *Apteronotus albifrons*: sensory acquisition strategies and electrosensory consequences. *J Exp Biol* 202: 1195–1203, 1999.

Nolting A, Ferraro T, D'hoedt D, Stocker M. An amino acid outside the pore region influences apamin sensitivity in small conductance Ca^{2+}-activated K^+ channels. *J Biol Chem* 282: 3478–3486, 2007.

Oswald A-MM, Chacron MJ, Doiron B, Bastian J, Maler L. Parallel processing of sensory input by bursts and isolated spikes. *J Neurosci* 24: 4351–4362, 2004.

Passaglia C, Troy JB. Information transmission rates of cat retinal ganglion cells *J Neurophysiol* 91: 1217–1229, 2004.

Rashid AJ, Dunn RJ, Turner RW. A prominent soma-dendritic distribution of Kv3.3 K^+ channels in electrosensory and cerebellar neurons. *J Comp Neurol* 441: 234–247, 2001.

Rieke F, Warland D, de Ruyter van Steveninck RR, Bialek W. *Spikes. Exploring the Neural Code.* Cambridge, MA: MIT Press, 1996.

Roddey JC, Girish B, Miller JP. Assessing the performance of neural encoding models in the presence of noise. *J Comput Neurosci* 8: 95–112, 2000.

Saunders J, Bastian J. The physiology and morphology of two types of electrosensory neurons in the weakly electric fish, *Apteronotus leptorhynchus. J Comp Physiol [A]* 154: 199–209, 1984.

Scheich H, Bullock TH, Hamstra RHJ. Coding properties of two classes of afferent nerve fibers: high frequency electroreceptors in the electric fish, *Eigenmannia. J Neurophysiol* 36: 39–60, 1973.

Shumway C. Multiple electrosensory maps in the medulla of weakly electric gymnotiform fish. I. Physiological differences. *J Neurosci* 9: 4388–4399, 1989a.

Shumway C. Multiple electrosensory maps in the medulla of weakly electric gymnotiform fish. II. Anatomical differences. *J Neurosci* 9: 4400–4415, 1989b.

Tan EW, Nizar JM, Carrera EG, Fortune ES. Electrosensory interference in naturally occurring aggregates of a species of weakly electric fish, *Eigenmannia virescens. Behav Brain Res* 164: 83–92, 2005.

Turner RW, Plant JR, Maler L. Oscillatory and burst discharges across electrosensory topographic maps. *J Neurophysiol* 76: 2364–2382, 1996.

Van Essen DC, Gallant JL. Neural mechanisms of form and motion processing in the primate visual system. *Neuron* 13: 1–10, 1994.

Wang X-J. Calcium coding and adaptive temporal computation in cortical pyramidal neurons. *J Neurophysiol* 79: 1549–1566, 1998.

Wässle H. Parallel processing in the mammalian retina. *Nat Rev Neurosci* 5: 1–11, 2004.

Zakon HH, Oestreich J, Tallarovic SK, Triefenbach F. EOD modulations of brown ghost electric fish: JARs, chirps, rises, and dips. *J Physiol* 96: 451–458, 2002.

Zupanc GK, Airey JA, Maler L, Sutko JL, Ellisman MH. Immunohistochemical localization of ryanodine binding proteins in the central nervous system of gymnotiform fish. *J Comp Neurol* 325: 135–151, 1992.

Zupanc GKH, Maler L. Evoked chirping in the weakly electric fish *Apteronotus leptorhynchus*: a quantitative biophysical analysis. *Can J Zool* 71: 2301–2310, 1993.

Zupanc GKH, Sirbulescu RF, Nichols A, Ilies I. Electric interactions through chirping behavior in the weakly electric fish, *Apteronotus leptorhynchus. J Comp Physiol [A]* 192: 159–173, 2006.